



Chemical Physics Impact

Volume 7, December 2023, 100385

Full Length Article

Synthesis, GCMS, spectroscopic, electronic properties, chemical reactivity, RDG, topology and biological assessment of 1-(3,6,6-trimethyl-1,6,7,7a-tetrahydrocyclopenta[c]pyran-1-yl)ethanone

E. Dhanalakshmi ^a  , P. Rajesh ^a  , K. Arunkumar ^b, T. Gnanasambandan ^c,
Noureddine ISSAOUI ^d, K. Sudha ^e, M. Raja ^f

[Show more](#) 

 Outline |  Share  Cite

<https://doi.org/10.1016/j.chphi.2023.100385> 

[Get rights and content](#) 

Under a Creative Commons [license](#) 

open access

Highlights

- The synthesised 1-(3,6,6-Trimethyl-1,6,7,7a-tetrahydrocyclopenta[c]pyran-1-yl) ethanone compound was conformed in GCMS– results.
- The spectral characterisations of FT-IR and UV–vis results correlated with DFT calculation.

- Energy gap, UV-vis and MEP was performed in solute-solvent interactions estimated by B3LYP/6-311G(d,p) method.
- The ELF, LOL, RDG, Fukui, drug-likeness on TTCPE was calculated.
- Docking result exhibit good binding affinity against anti-cancer activity.

Abstract

The inclusion of the majority of heterocycle fragments in the pharmaceutical arena currently on drug discovery, combined with their inherent adaptability and distinctive physicochemical features, has established them as true pillars of therapeutic/medicinal chemistry. Besides from the medications, numerous others are being researched for their potential anti-carcinogenic behavior. In this current study, a newly synthesized TTCPE molecular structure from carbinol extract of Aeglemarmelos leaves has been confirmed by GC-MS results, and structural characteristics are reported. The quantum chemical simulated calculations were employed using a versatile basis set -B3LYP/6-311++G(d,p) approach. The optimized structure with the minimum energy confirmation was carried out using Potential scan energy (PES) analysis and the optimized with atom numbering scheme of TTCPE discovered strength of the bond parameters and compared with XRD data. Experimental and theoretical spectral characterizations were accomplished and the vibrational wavenumbers provide an affordable correlation with the experimental value. The UV-vis electronic spectra associated with the gas phase and various solvent-liquid phases were obtained by TD-SCF methods. The high stabilization energy $E(2)$ value is 128.06kcal/mol executed by the NBO method along with the lone pair of interaction types in the header composite. The MEP map, HOMO-LUMO- intermolecular charge transfer (ICT) was completed by gas and different solvents and their corresponding energy parameters were evaluated. Fukui function describes reactive sites on TTCPE that were investigated. The topological analysis of LOL, ELF, and RDG was performed. The five principles of Lipinski are used to perform drug-likeness qualities. Furthermore, a molecular docking technique was used to compare ligand to several protein inhibitor targets (1H8X, 6R7T, and 6DX5) and the corresponding parameters were calculated. As a result, the header composite identifies an alternative anticancer treatment agent.

Graphical abstract



[Download: Download high-res image \(256KB\)](#)

[Download: Download full-size image](#)

[<](#) Previous

Next [>](#)

Keywords

GC-MS, FT-IR; UV-visible; Topological properties, drug-likeness; Docking studies

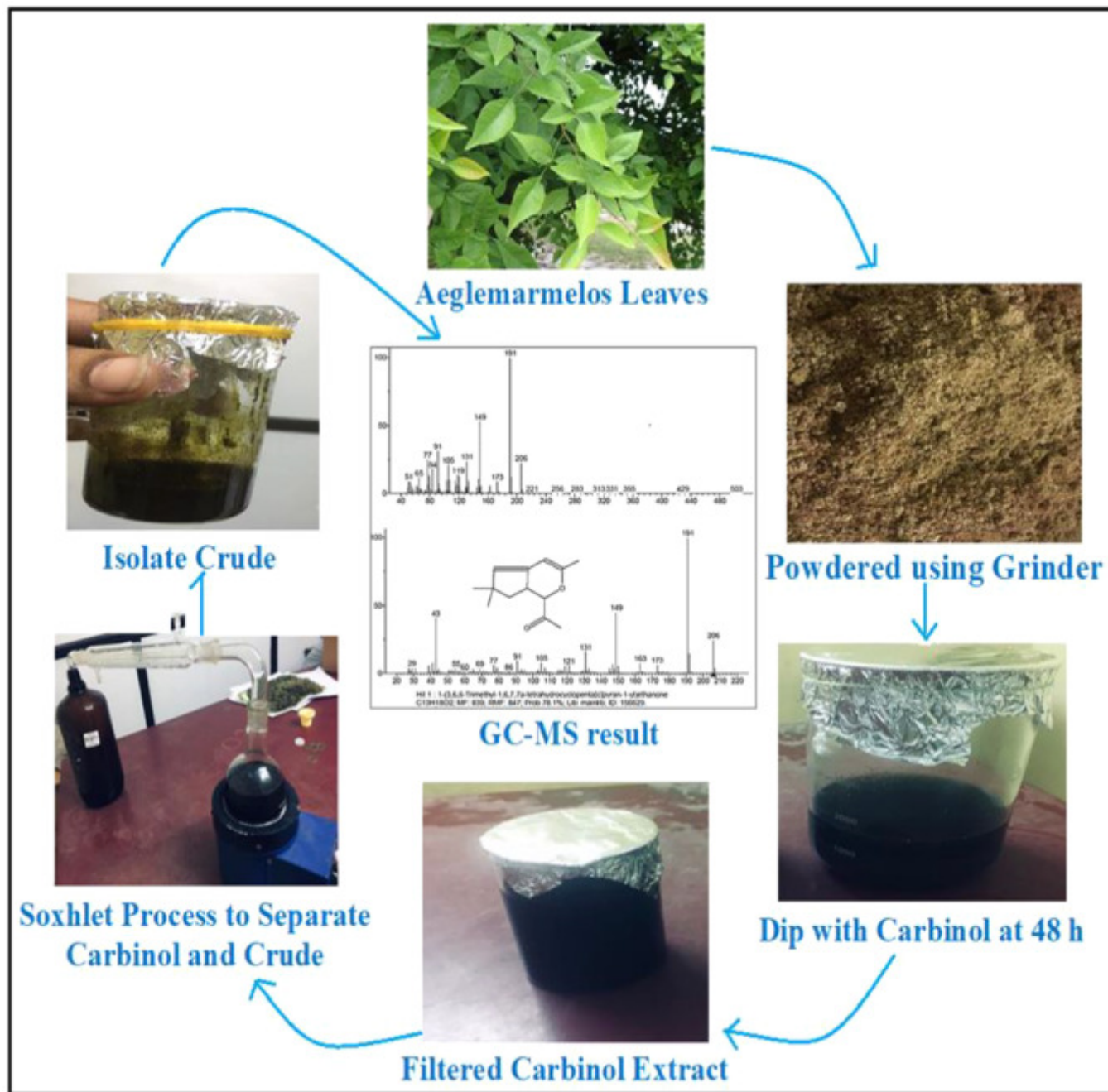
1. Introduction

Globally, the cancer is one of the most affected by pancreatic (12.2%), melanoma (12.5%) and ovarian (10.7%) reported by world health organization. That cancer activity compound naturally synthesis from *Aeglemarmelos leaves* and The literature survey revealed *Aeglemarmelos leaves* belongs to Rutaceae family, it's also called Vilvam in Tamil, Beal in Hindi and Bilva in Sanskrit which is global plat and provide biologically active compounds such has fibers, carotenoids, phenolics, terpenoids, coumarins, flavonoids, and alkaloids. The leaf extract useful for cure inflammation, tuberculosis, treating fever, antibacterial, antiviral and anti-ulcerative colitis [1]. The TTCPE molecules synthesized from *Aeglemarmelos leaves*, that molecular formula $C_{13}H_{18}O_2$ and molecular weight 206g. the green synthesized of title molecule trimethyl and derivatives related to breast, lung, ovarian, melanoma, breast, pancreatic and colon cancer, respectively [2,3]. neuroprotective potential [4], pharmacological and ethno-medicinal [5], antibacterial activity and phytochemical potential [6], The biochemical alterations in the therapy of diabetes are estimated using the methanol extract of *A. marmelos leaves* [7], the ethanolic extract of *Aeglemarmelos leaves*

was used to test for antioxidant activity using GC–MS, NMR, and HPLC [8], The nanocomposite synthesised from waste leaf of *A. marmelos* investigated by XRD, TEM, FESEM, BET and VSM [9], the leaves extract from different solvent analysis antioxidant activity through DPPH and CV methods [10], the silver nanoparticles biosynthesis from aqueous leaf extract examination of anticancer, larvicidal activity [11]. The best of our knowledge, based on the above research work reported the density functional calculation (DFT) not yet been carried out. The main objective of the present work report the GC–MS analysis crude of *Aeglemarmelos leaves* which result report TTCPE compound for structure conformation. The optimized structure properties, the simulated FT-IR and UV–vis spectra performed by B3LYP/6-311++G(d,p) process and correlated with infrared data on TTCPE molecules. NBO study, MEP surface, Fukui function, PES scan and energy gap reported well biological activity was interpreted by DFT. Topological parameter, RDG investigation and Lipinski's rules calculated physical-chemical characteristics showed good features of drug-likeness were also computed. The docking studies revealed good ligand-protein interaction on TTCPE molecules against Anti-cancer activity.

2. Green synthesis of the *Aeglemarmelos leaves* plant

The *Aeglemarmelos leaves* have collected from kalyanakuppam village, Tiruvallur, Tamil Nadu, India. The 100% medicinal plant *Aeglemarmelos leaves* at 3 kg were washed with fresh water, which takes 25 to 30 days to dry at normal temperature. Furthermore, Preserved portion of 1 kg has given into grinder to made fine powder, which power dip with 95.5% carbinol (2:1 ratio) keep 48 h at room temperature to observe components. The Whatman filter paper used to filtered leaf extract for qualitative analysis, which solvent used soxhlet process to isolate carbinol and crude. The preparation of carbinol extract of *Aeglemarmelos leaves* as given in [Scheme 1](#), respectively [12].



Download: [Download high-res image \(994KB\)](#)

Download: [Download full-size image](#)

Scheme 1. Identified TTCPE compound from crude of *Aeglemarmelos leaves*.

2.1. Experimental techniques details

The crude were investigate the Gas chromatography – mass spectrometry (GC–MS) technique (QP2010 Plus – Shimadzu) The MS non-polar capillary column, which has a 30m length, 0.25mm inner diameter, and 0.25m thickness, is coated with polydimethylsiloxane, continued to inject 250°C temperature and GC–MS spectra exhibit region 25min. The GC–

MS result recorded multiple bio-compounds, particularly we choose one quantitative phytochemical compound (TTCPE) based on anti-cancer activity for further studies and 99% pure TTCPE chemical was bought from the Sigma-Aldrich Company. FT-IR spectrum analysis used to evaluate the TTCPE sample in the recorded area $4000 - 400\text{cm}^{-1}$. The spectrum was measured at room temperature using a Perkin Elmer FT-IR spectrophotometer with KBr pellet method and the spectral solution containing 4.0cm^{-1} . The UV-vis spectrum has been observed wavelength area from 300 – 100nm with UV-3600 plus Shimadzu Instrument employs a quartz cell with a 1 cm diameter and a slit width of 0.5 nm. GC-MS, FT-IR and UV-vis spectrum results were recorded at the SRM College of Science in Kattankulathur, Chengalpattu district, Tamil Nadu, India.

3. Computational details

In this study, the computational investigate of TTCPE molecular structure has been obtained by DFT technique using hybrid functional Becke-3-Lee-Yang-Parr (B3LYP) parallel with 6-311++G(d,p) program [13,14]. The geometry molecular structure, HOMO-LUMO, PES scan and MEP illustrated through by GaussView 5.0 and ChemCraft 1.8 tools [15,16]. The structural conformational through PES scan, optimized geometrical properties, MEP plot and Fukui function characterization with NPA charges on TTCPE molecules interpreted B3LYP/6-311++G(d,p) technique. The basic harmonics frequency was scaled by a factor of 0.963 with PED% interpreted using Veda 04 program, which exhibit well correlated with the experiment spectra. The gas and various solvent of UV-vis spectra have been determined using TD-SCF process. On the basis of Koopmans equation, the HOMO-LUMO energy gap and chemical reactivity indices were obtained by using molecular orbital analysis. NBO analysis of intra-inter molecular interaction between bonding, antibonding and high stabilization energy values are carried out NBO 3.1 software [17,18]. The topological parameters of RDG, ELF and LOL have been computed by MULTIWFN 3.7 bin Win 64 software [19]. The AutoDock 1.5.6 programme has interpreted the molecular docking of ligand-protein binding energy [20].

4. Results and discussion

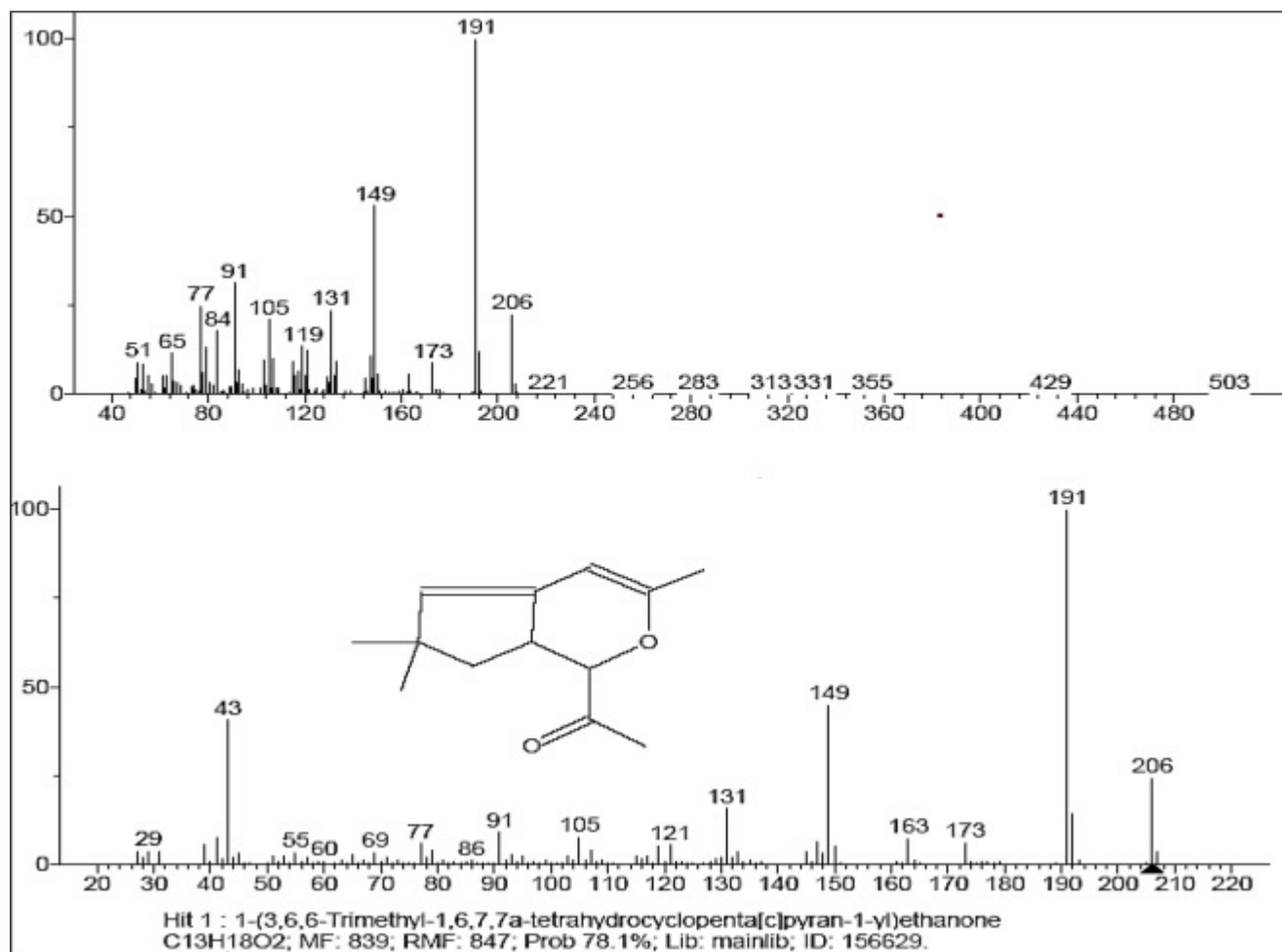
4.1. GC-MS examination on carbinol extract of *Aeglemarmelos leaves*

The GC-MS technique was investigate carbinol cuude of *Aeglemarmelos Leave*, which reported various pharmaceutical components are given in [Table 1 \[21\]](#). That bio-compound identify by based on comparing with related retention time, molecular formula, molecular weight and database from NIST library [22]. The GC-MS result exhibit totally five

compounds namely, 3-O-methyl-d-glucose, Behenic acid, 1-(3,6,6-Trimethyl-1,6,7,7a-tetrahydrocyclopenta[c]pyran-1-yl)ethanone (TTCPE), 2(4H)-Benzofuranone, 5,6,7,7a-tetrahydro-4,4,7a-trimethyl-, (*R*)-, 3-Buten-2-one, 4-(4-hydroxy-2,2,6-trimethyl-7-oxabicyclo[4.1.0]hept-1-yl)- those bio components are conformed based on molecular formula ($C_7H_{14}O_6$, $C_{22}H_{44}O_2$, $C_{13}H_{18}O_2$, $C_{11}H_{16}O_2$ and $C_{13}H_{20}O_3$, molecular weight (261.08, 340.6, 206.28, 180.24 and 224.30g/mol) and retention time (18.26, 21.03, 22.14, 24.98 and 25.87). Several components were reported by the GC-MS; however we selected only one bio-compound, TTCPE, because it has more closely associated anti-cancer activity. [23] as shown in Fig. 1. We have performed spectrum analysis on TTCPE compound using FT-IR, UV-vis, and DFT, as well as molecular docking against Anti-cancer activity.

Table 1. Bioactive components synthesis from *Aeglemarmelos leaves*.

Name of the Compound	Molecular Formula	Molecular Weight (g/mol)	Retention time
3-O-methyl-D-glucose	$C_7H_{14}O_6$	261.08	18.26
Behenic acid	$C_{22}H_{44}O_2$	340.6	21.03
1-(3,6,6-Trimethyl-1,6,7,7a-tetrahydrocyclopenta[c]pyran-1-yl)ethanone	$C_{13}H_{18}O_2$	206.28	22.14
2(4H)-Benzofuranone, 5,6,7,7a-tetrahydro-4,4,7a-trimethyl-, (<i>R</i>)-	$C_{11}H_{16}O_2$	180.24	24.98
3-Buten-2-one, 4-(4-hydroxy-2,2,6-trimethyl-7-oxabicyclo[4.1.0]hept-1-yl)-	$C_{13}H_{20}O_3$	224.30	25.87



[Download: Download high-res image \(351KB\)](#)

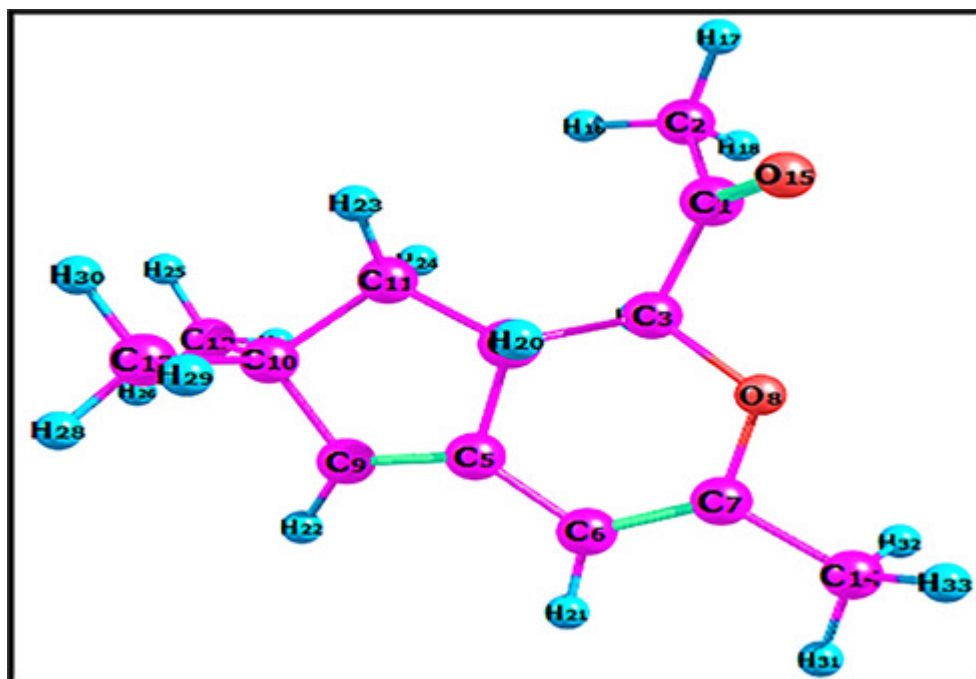
[Download: Download full-size image](#)

Fig. 1. GC–MS result on TTCPE compound.

4.2. Geometrical parameters and pes scan analysis

The green syntheses of TTCPE molecules optimized by visualize using GaussView 5.0 software as displayed in Fig.2. Geometry optimized properties of bond distance and bond angle interpreted B3LYP/6- 311++G (d, p) technique as seen in Table2 [24,25]. These bond parameters provide useful information on a chemical compound's stability and its effectiveness of the bonds of molecules that keep its atoms connected. According to covalent bond (single bond > double bond > triple bond) shared electrons of single bond has one shared pair, double bond has two shared pair and three bond has triple bond pair. The number of shared pair of electrons increased attraction of strength, stability and decreased distance between bonds, therefore low electron pair → longer bond distance + less bond strength and many electron pair → small bond distance + high bond strength on the molecular system [26]. In the present investigation on title molecules contain five double

bonds and 29 single bonds, from C=C bonds exhibit $C_6-C_7 \rightarrow 1.353$, $C_5-C_9 \rightarrow 1.344$ and $C_5-C_6 \rightarrow 1.444 \text{ \AA}$ those bond distance values are smallest distance+high strongest bond and greater than C—C bonds express $C_{10}-C_{13} \rightarrow 1.545$, $C_{10}-C_{12} \rightarrow 1.538$ and $C_{10}-C_{11} \rightarrow 1.564 \text{ \AA}$ these bond distances indicate highest distance+less strongest bonds ($C=C > C-C$) on the TTCPE. Similarly, the C=O bond express $C_1-O_{15} \rightarrow 1.213$ and $C_7-O_8 \rightarrow 1.268 \text{ \AA}$ both are short distance+highest stability bond and C—O bond reveal $C_3-O_8 \rightarrow 1.436 \text{ \AA}$, which is long distance+lowest stability bond that C=O greater than C—O ($C=O > C-O$) on title compound, respectively. Therefore, the calculated optimized parameter of theoretical values compared with experimental (XRD) of crystallographic data [27]. The chemical calculation of bond distance C_5-C_9 , C_9-C_{10} , $C_{10}-C_{11}$, C_4-C_{11} , $C_{10}-C_{12}$ and C_4-C_5 1.344 appear values 1.344, 1.521, 1.564, 1.541, 1.538 and 1.517 \AA correlated with XRD bond distance 1.360, 1.492, 1.568, 1.571, 1.507 and 1.497 \AA . determined angle of bond $C_{10}-C_{13}-H_{29}$, $C_{10}-C_{13}-H_{30}$ exhibit values 111.314, 111.027° corresponding with experimental bond angle 111.5 and 111.5 ° both shows well correlated with the XRD and theoretical estimates in tetrahydro on TTCPE compound successively [28,29]. The conformational flexibility of TTCPE structure have been performed through PES scan surface computed by HF/6-311++G (d, p) program [30]. The torsion angle of $O_{15}-C_1-C_3-H_{19}$ in tetrahydro find stability and instability in the TTCPE molecules based on the local minimum energy occurred in the PES scan plot report as shown Fig.3 [31,32]. The dihedral angle of title molecules rotate around each step scan at 10° with 360° degree revealed multiple conformers. Amongst the all conformations, local minimum energy curve with -0.099 total energy (Hartree) was seen at the 100° scan coordinator, indicating a more stable conformation. The torsional angle ($O_{15}-C_1-C_3-H_{19}$) of the local maximum energy curve, which conformed at -110° scan coordinator with -0.096 Hartree energy, indicates a less stable conformation on TTCPE molecules.



[Download: Download high-res image \(285KB\)](#)

[Download: Download full-size image](#)

Fig. 2. Optimized molecular structure on TTCPE molecules.

Table 2. Low and high stability of bond angle, length on TTCPE compound.

Bond length (Å)	B3LYP /6-311++G(d,p)	Experimental Data	Bond Angle (°)	B3LYP /6-311++G(d,p)	Experimental Data
(C ₁ —C ₂)	1.514	1.51	(C ₃ —C ₄ —C ₅)	108.889	—
(C ₁ —C ₃)	1.535	1.56	(C ₃ —C ₄ —C ₁₁)	117.883	117.95
(C ₁ —O ₁₅)	1.213	1.22	(C ₃ —C ₄ —H ₂₀)	106.007	—
(C ₂ —H ₁₆)	1.095	1.00	(C ₅ —C ₄ —C ₁₁)	102.890	—
(C ₂ —H ₁₇)	1.090	—	(C ₅ —C ₄ —H ₂₀)	109.719	—
(C ₂ —H ₁₈)	1.096	—	(C ₁₁ —C ₄ —H ₂₀)	111.311	111.5

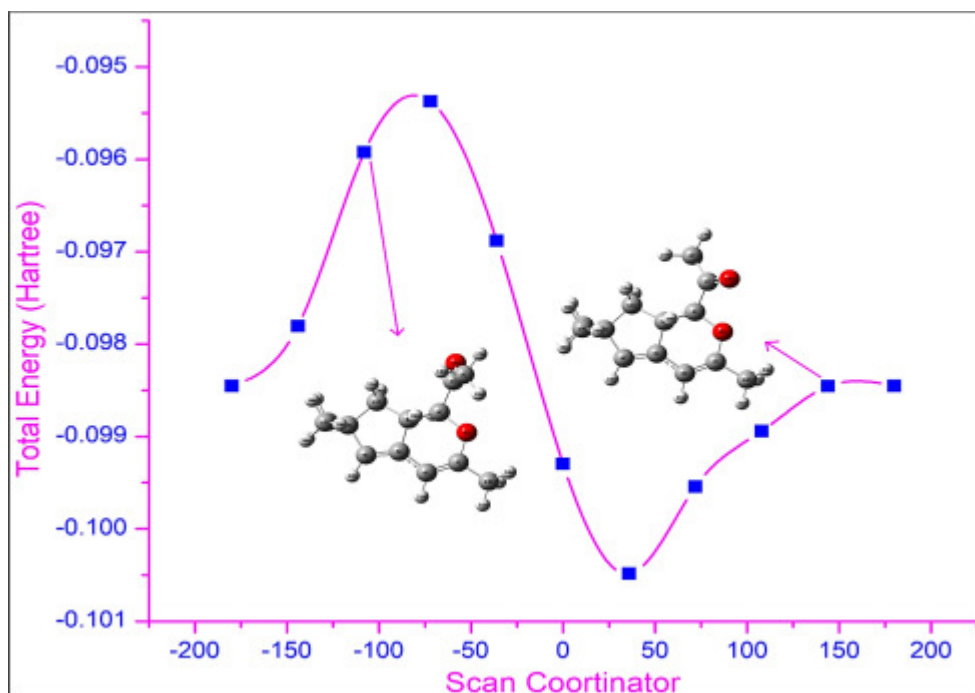
Bond length (Å)	B3LYP /6-311++G(d,p)	Experimental Data	Bond Angle (°)	B3LYP /6-311++G(d,p)	Experimental Data
(C ₃ —C ₄)	1.537	1.57	(C ₄ —C ₅ —C ₆)	116.692	117.39
(C ₃ —O ₈)	1.436	1.43	(C ₄ —C ₅ —C ₉)	110.613	111.1
(C ₃ —H ₁₉)	1.102	–	(C ₆ —C ₅ —C ₉)	132.692	–
(C ₄ —C ₅)	1.517	1.50	(C ₅ —C ₆ —C ₇)	119.817	119.54
(C ₄ —C ₁₁)	1.541	1.57	(C ₅ —C ₆ —H ₂₁)	121.063	120.2
(C ₄ —H ₂₀)	1.099	–	(C ₇ —C ₆ —H ₂₁)	119.110	119.4
(C ₅ —C ₆)	1.444	1.40	(C ₆ —C ₇ —O ₈)	123.531	125.19
(C ₅ —C ₉)	1.344	1.39	(C ₆ —C ₇ —H ₁₄)	125.591	–
(C ₆ —C ₇)	1.353	1.39	(C ₈ —C ₇ —H ₁₄)	110.876	111.5
(C ₆ —H ₂₁)	1.084	–	(C ₃ —O ₈ —C ₇)	117.627	–
(C ₇ —O ₈)	1.268	1.22	(C ₅ —C ₉ —H ₁₀)	112.725	–
(C ₇ —C ₁₄)	1.495	1.49	(C ₅ —C ₉ —H ₂₂)	125.150	–
(C ₉ —C ₁₀)	1.521	1.51	(C ₁₀ —C ₉ —H ₂₂)	122.100	120.2
(C ₉ —H ₂₂)	1.087	0.95	(C ₉ —C ₁₀ —C ₁₁)	101.272	

Bond length (Å)	B3LYP /6-311++G(d,p)	Experimental Data	Bond Angle (°)	B3LYP /6-311++G(d,p)	Experimental Data
(C ₁₀ —C ₁₁)	1.564	–	(C ₉ —C ₁₀ —C ₁₂)	112.30	–
(C ₁₀ —C ₁₂)	1.538	–	(C ₉ —C ₁₀ —C ₁₃)	110.754	109.05
(C ₁₀ —C ₁₃)	1.545	–	(C ₁₁ —C ₁₀ —C ₁₂)	111.874	–
(C ₁₁ —H ₂₃)	1.094	0.98	(C ₁₁ —C ₁₀ —C ₁₃)	111.117	–
(C ₁₁ —H ₂₄)	1.098	0.98	(C ₁₂ —C ₁₀ —C ₁₃)	109.345	–
(C ₁₂ —H ₂₅)	1.096	0.98	(C ₄ —C ₁₁ —C ₁₀)	105.145	–
(C ₁₂ —H ₂₆)	1.095	0.95	(C ₄ —C ₁₁ —H ₂₃)	113.381	–
(C ₁₂ —H ₂₇)	1.095	0.95	(C ₄ —C ₁₁ —H ₂₄)	109.432	–
(C ₁₃ —H ₂₈)	1.095	0.98	(C ₁₀ —C ₁₁ —H ₂₃)	112.558	111.5
(C ₁₃ —H ₂₉)	1.094	0.98	(C ₁₀ —C ₁₁ —H ₂₄)	108.634	–
(C ₁₃ —H ₃₀)	1.096	0.98	(H ₂₃ —C ₁₁ —H ₂₄)	107.591	–
(C ₁₄ —H ₃₁)	1.091	0.98	(C ₁₀ —C ₁₂ —H ₂₅)	111.012	111.5
(C ₁₄ —H ₃₂)	1.095	0.98	(C ₁₀ —C ₁₂ —H ₂₆)	111.026	111.5
(C ₁₄ —H ₃₃)	1.095	0.98	(C ₁₀ —C ₁₂ —H ₂₇)	111.149	111.5

Bond length (Å)	B3LYP /6-311++G(d,p)	Experimental Data	Bond Angle (°)	B3LYP /6-311++G(d,p)	Experimental Data
Bond Angle (°)	B3LYP /6-311++G(d,p)		(H ₂₅ —C ₁₂ —H ₂₆)	107.515	—
(C ₂ —C ₁ —C ₃)	116.668	117.39	(H ₂₅ —C ₁₂ —H ₂₇)	108.135	—
(C ₂ —C ₁ —O ₁₅)	122.799	—	(H ₂₆ —C ₁₂ —H ₂₇)	107.850	—
(C ₃ —C ₁ —O ₁₅)	120.512	—	(C ₁₀ —C ₁₃ —H ₂₈)	110.805	—
(C ₁ —C ₂ —H ₁₆)	110.979	—	(C ₁₀ —C ₁₃ —H ₂₉)	111.314	111.5
(C ₁ —C ₂ —H ₁₇)	109.852	109.5	(C ₁₀ —C ₁₃ —H ₃₀)	111.027	111.5
(C ₁ —C ₂ —H ₁₈)	109.630	109.5	(H ₂₈ —C ₁₃ —H ₂₉)	107.607	—
(H ₁₆ —C ₂ —H ₁₇)	110.029	109.5	(H ₂₈ —C ₁₃ —H ₃₀)	107.747	—
(H ₁₆ —C ₂ —H ₁₈)	106.783	—	(H ₂₉ —C ₁₃ —H ₃₀)	108.187	—
(H ₁₇ —C ₂ —H ₁₈)	109.509	109.5	(C ₇ —C ₁₄ —H ₃₁)	110.934	—
(C ₁ —C ₃ —C ₄)	111.502	—	(C ₇ —C ₁₄ —H ₃₂)	110.768	—
(C ₁ —C ₃ —O ₈)	106.665	—	(C ₇ —C ₁₄ —H ₃₃)	110.121	—
(C ₁ —C ₃ —H ₁₉)	110.667	111.5	(H ₃₁ —C ₁₄ —H ₃₂)	109.097	109.5
(C ₄ —C ₃ —O ₈)	110.512	—	(H ₃₁ —C ₁₄ —H ₃₃)	108.817	109.5

Bond length (Å)	B3LYP /6-311++G(d,p)	Experimental Data	Bond Angle (°)	B3LYP /6-311++G(d,p)	Experimental Data
(C ₄ —C ₃ —H ₁₉)	109.177	111.5	(H ₃₂ —C ₁₄ —H ₃₃)	106.998	—
(O ₈ —C ₃ —H ₁₉)	108.247	109.5			

RMSD value of bond length - 0.0562Å, RMSD value of bond angles - 0.0892°.



Download: [Download high-res image \(297KB\)](#)

Download: [Download full-size image](#)

Fig. 3. Potential energy surface curve of TTCPE.

4.3. Vibrational assignments

The vibrational spectroscopy provides individual fundamental vibrations that used to demonstrating the structure of molecules and is a great method for quick and precise measurement by organic chemistry. In the present investigation, the harmonic vibrational modes of TTCPE molecules contain 33 atom and the result of 93 normal modes found through FT-IR spectrum [33,34]. The calculated vibrational assignments of TTCPE interpreted at B3LYP level 6-311++G(d,p) basis with PED% performed by using VEDA 04 and

the scaled rate of 0.963 compute in the Table 3 [35,36]. The observed and experimentally recorded spectra are well correlated on TTCPE molecules have been shown in Fig. 4 successively. Normally, the methyl asymmetric and symmetric groups are found between 3120 – 3060, 3025 – 3015 cm^{-1} [37]. Asymmetry CH_3 stretching vibrational appears in the area 3166 and 3149 cm^{-1} with 84% PED in calculated spectra and the FT-IR spectrum of CH_3 in TTCPE compound with the greatest intensity emerge in the region between 3168 and 3152 cm^{-1} . The CH_3 symmetric stretching oscillations happen at 3044, 3030 cm^{-1} with 72% PED was computed theoretically and the CH_3 group arise 3035, 3032 cm^{-1} in FT-IR spectra. The CH_2 $\nu(\text{s})$ and $\nu(\text{as})$ stretching is belongs to the bands expressed 3000 – 2900 cm^{-1} [38]. The CH_2 asymmetric stretching vibration absorption showed 3103, 3099 and 3092 cm^{-1} in FT-IR spectra and computational spectra of CH_2 asymmetric stretching seem at 3100, 3099 and 3093 cm^{-1} with 99% PED. The CH_2 symmetric frequencies exhibit area 3025 cm^{-1} with extreme intensity in FT-IR spectra and recorded spectra range 3026 cm^{-1} with 84% PED. According to a literature review, the active C=O oscillation frequency was reported to be around 1800–1600 cm^{-1} [39]. The FT-IR spectra, the C=O band vibration on the title compound appeared area at 1828 cm^{-1} and corresponding DFT calculation interpreted B3LYP/6-311++G(d,p) set at area 1828 cm^{-1} with 91% PED. The C—O oscillating frequency occurred between 1260 and 1000 cm^{-1} [40]. In the FT-IR spectra, the C—O oscillation frequency appeared across 1193, 1089 cm^{-1} with a medium intensity and computed C—O oscillation frequency appears area at 1196, 1084 cm^{-1} with lowest PED%. The out of plane γOCCC bands occurred in the range at 1032, 612 cm^{-1} in the FT-IR spectra and the calculated spectra of γOCCC frequency region at 1034, 608 with minimum PED degree. The C—C oscillating frequency occurs 1590 - 1000 cm^{-1} [41]. Frequency bands of C—C oscillations can be seen at 1379, 1283, 1234, 1193, 1109, 1057 and 1015 cm^{-1} with min to max intensity in spectrum of FT-IR. The simulated spectra of νCC band exhibit area 1375, 1294, 1228, 1188, 1104, 1051 and 1017 cm^{-1} with mixed PED 14.5%. The C—H occurred between 3250 – 2950 cm^{-1} [42]. The C—H band vibrations appear at 3206 cm^{-1} with minimum intensity in the infrared spectrum and theoretical prediction of C—H stretching frequency observed band at 3207 cm^{-1} with corresponding PED 99% in the TTCPE compound. All spectrum data collected from theoretical and experimental frequencies are contrast and found to be in good agreement.

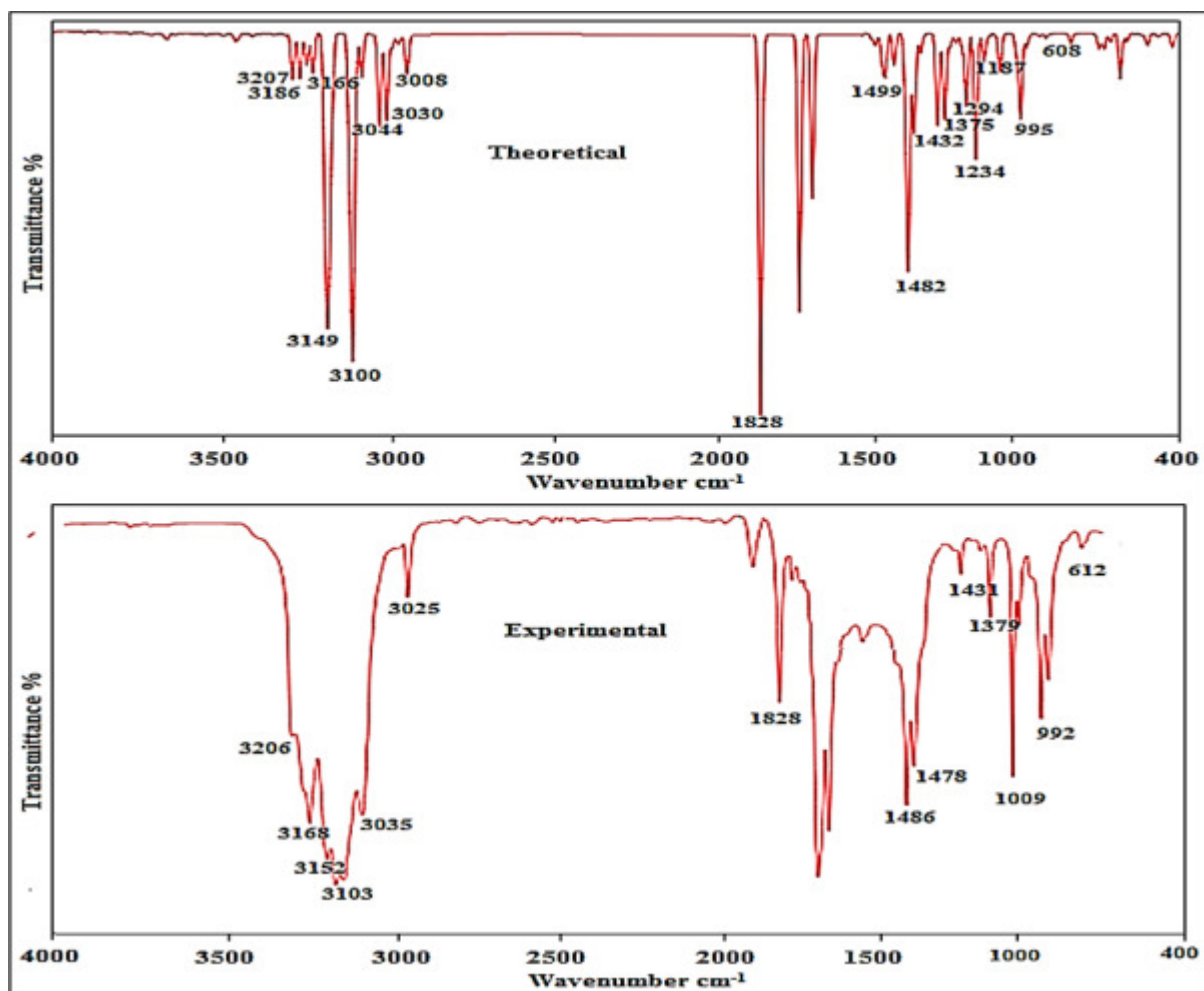
Table 3. Simulated experimental and theoretical frequencies on TTCPE.

B3LYP/6-311++G (d, p)	Experimental cm^{-1}	Vibrational Assignments+(PED%)
Scaled	FT-IR	
3207	3206	νCH (99)

B3LYP/6-311++G (d, p)	Experimentalcm^{-1}	Vibrational Assignments+(PED%)
Scaled	FT-IR	
3186	–	νCH (99)
3166	3168	τCH_3 (84)
3149	3152	τCH_3 (83)
3115	–	νCH_3 (55)
3110	–	νCH_3 (46)
3104	–	νCH_2 (74)
3100	3103	νCH^2 (53)
3099	3099	νCH_2 (96)
3093	3092	νCH_2 (75)
3044	3035	νCH_3 (97)
3030	3032	νCH_3 (48)
3026	3025	νCH_2 (84)
3008	3012	νCH (98)
1828	1828	νOC (91)
1716	–	νCC (56)+ δCCC (15)
1680	–	νCC (46)
1521	–	δHCH (51)
1516	–	δHCH (42)
1506	–	δHCH (35)
1500	–	δHCH (50)+ HCCC (23)
1499	–	δHCH (40)
1495	–	δHCH (42)
1487	1486	δHCH (53)+ HCCC (14)
1482	–	δHCH (43)+ HCCC (10)
1475	1478	δHCH (45)

B3LYP/6-311++G (d, p)	Experimentalcm^{-1}	Vibrational Assignments+(PED%)
Scaled	FT-IR	
1432	1431	δHCH (52)
1429	–	δHCH (44)
1409	–	δHCH (51)
1405	–	δHCO (31)
1392	–	δHCH (58)+ δHCO (11)
1375	1379	νCC (16)+ τHCOC (16)+ τHCCC (15)
1365	–	δHCO (13)+ δCCC (13)+ τHCCC (21)
1354	–	δHCC (19)+ τHCOC (17)
1336	–	δHCC (34)+ δHCO (15)+ τHCCC (22)
1294	1292	νCC (17)+ δHCC (13)
1282	1283	δHCC (27)+ νCC (17)
1263	–	δHCC (16)+ τHCCC (12)
1228	1234	νCC (14)+ δHCC (14)
1196	1193	νOC (18)+ νCC (20)
1188	1187	νCC (12)+ δOCC (11)+ τHCOC (15)
1171	–	δHCC (44)
1153	–	τHCCC (14)
1104	1109	νCC (13)+ δCCC (12)
1084	1089	νOC (25)
1069	–	δHCH (27)+ τHCCC (51)
1051	1057	νCC (19)
1034	1032	τHCCC (27)+ γOCCC (14)
1022	–	τHCCC (10)
1017	1015	νCC (11)
995	992	νCC (11)

B3LYP/6-311++G (d, p)	Experimentalcm^{-1}	Vibrational Assignments+(PED%)
Scaled	FT-IR	
971	–	ν_{CC} (17)+ τ_{HCCC} (11)
958	–	ν_{CC} (10)+ τ_{HCCC} (12)
936	–	ν_{CC} (26)
920	921	ν_{CC} (33)
878	–	ν_{CC} (19)+ τ_{HCCC} (10)
866	–	τ_{HCCC} (67)
848	–	ν_{CC} (16)
813	815	τ_{HCCC} (48)
793	–	ν_{CC} (18)+ δ_{CCC} (27)
722	–	ν_{CC} (19)+ δ_{OCC} (11)
641	–	τ_{OCCC} (11)+ τ_{CCCC} (15)
627	–	ν_{CC} (11)+ δ_{OCC} (12)
608	612	τ_{HCCC} (21)+ γ_{OCCC} (24)



Download: [Download high-res image \(528KB\)](#)

Download: [Download full-size image](#)

Fig. 4. FT-IR simulated spectrum of TTCPE.

4.4. Electronic properties

4.4.1. FMO analysis on TTCPE molecules

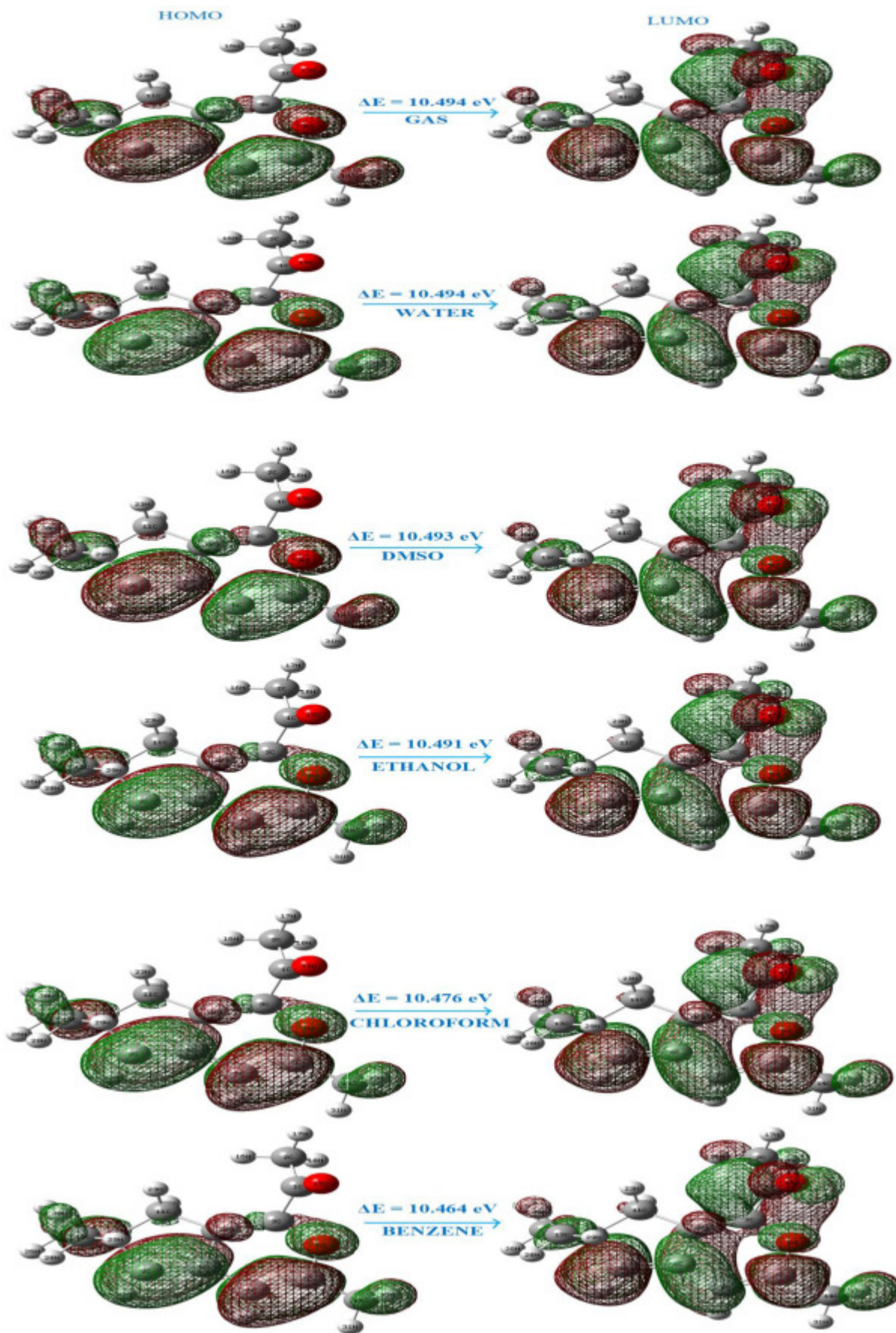
Quantum chemical parameters of E_H , E_L , ΔE , IP , EA , Electronegativity (χ), Chemical Potential (μ), Chemical Hardness (η), EDP (ω^+), EAP (ω^-) eV, Chemical Softness (σ), Electrophilicity Index (ω), are performed by Gaussian 09W program using hybrid functional method DFT/B3LYP/6-311++G(d,p) basis set computed with gas phase and different solvents are given in [Table 4](#). On the basis of Koopmans equation [43] the HOMO, LUMO have been optimized to visualized using GaussView 05 software illustrate in [Fig. 5](#) and the above properties are describes to given information about stability of chemical structure and chemical behavior on the title (TTCPE) molecules [44]. In the current investigation, the filled

orbital of nucleophilic consist electron pair to donate, due to more reaction involves while the empty orbital of electrophilic accept the electron pair which indicate formation of chemical bonds. Highest-energy filled molecular orbital of nucleophile values -7.640eV in gas and various solvent $-7.640, -7.638, -7.633, -7.597, -7.567\text{eV}$ donate pair of electrons has occupied in tetrahydrocyclopenta ring, due to less tightly connected electrons while lowest-energy filled molecular orbital of electrophilic values 2.854eV in gas and different solvent values $2.854, 2.855, 2.858, 2.878, 2.897$ are accept pair of electrons has unoccupied in ethanone structure, because minimum transition state and fastest reaction [45,46]. The ionization potential removes the electron from outer most orbital to form positive ion (cation) proportional to HOMO while electron affinity added the electron from neutral atom to form negative ion (anion) promotional to LUMO on the title molecules in different phases. The electronegativity describes the tendency of atoms difference between $IP+EA/2$ on the TTCPE molecules express 2.393eV in gas and $2.393, 2.391, 2.387, 2.359, 2.335\text{eV}$ in solvent, these values are represent attract stability of shared pair on electrons in covalent bond. If the electronegativity below 0.5 its non-polar covalent, the electronegativity 0.5 to 2.1 it's polar covalent and the electronegativity is above 2.1 it's indicate polar or ionic. The gas= 2.393eV , Water= 2.393eV both electronegativity are satisfied in polar or ionic covalent consists more reactive and stable compared than other solvents. The strong reaction is inversely correlated with low electrophilicity index energy value of 0.545eV and high nucleophilicity index energy value of 1.832eV of TTCPE molecules in gas and water phases, respectively [47]. The electron transition $\pi \rightarrow \pi^*$ and the high energy gap difference between HOMO, LUMO values in gas 10.494eV and in water 10.494eV , which represent low reactivity and high kinetic stability compared than other solvent on the TTCPE molecules its related to well biological activity [48].

Table 4. Electronic parameters on TTCPE molecules gas and solvent phases.

Molecular Parameters	Gas	Water	DMSO	Ethanol	Chloroform	Benzene
E_{HOMO} (eV)	-7.640	-7.640	-7.638	-7.633	-7.597	-7.567
E_{LUMO} (eV)	2.854	2.854	2.855	2.858	2.878	2.897
Ionization Potential (IP)	7.640	7.640	7.638	7.633	7.597	7.567
Electron Affinity (EA)	-2.854	-2.854	-2.855	-2.858	-2.878	-2.897
Energy gap (eV)	10.494	10.494	10.493	10.491	10.476	10.464
Electronegativity (χ)	2.393	2.393	2.391	2.387	2.359	2.335
Chemical Potential (μ)	-2.393	-2.393	-2.391	-2.387	-2.359	-2.335

Molecular Parameters	Gas	Water	DMSO	Ethanol	Chloroform	Benzene
Chemical Hardness (η)	5.247	5.247	5.246	5.245	5.238	5.232
Chemical Softness (σ)	0.095	0.095	0.095	0.095	0.095	0.095
Electrophilicity Index (ω)	0.545	0.545	0.545	0.543	0.531	0.521
Nucleophilicity index (N)	1.832	1.832	1.834	1.840	1.882	1.919
Electron Donor Power (ω^+)	2.398	2.398	2.396	2.392	2.365	2.342
Electron Acceptor Power (ω^-)	0.005	0.005	0.005	0.005	0.006	0.007



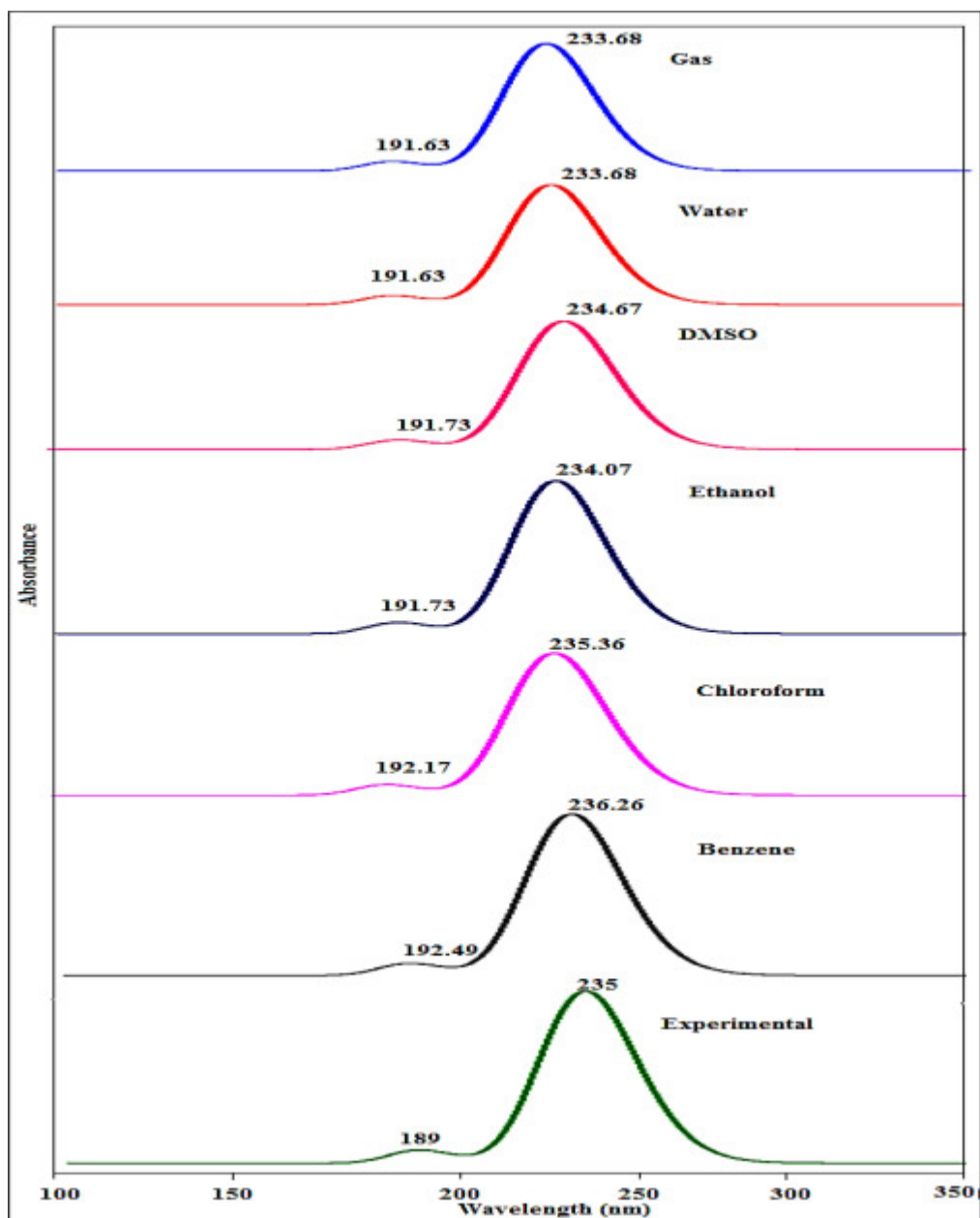
[Download: Download high-res image \(2MB\)](#)

[Download: Download full-size image](#)

Fig. 5. HOMO, LUMO illustrate and energy gap of TTECP in gas and solvents.

4.4.2. UV–visible absorption spectra

The UV–vis electronic spectra on TTCPE molecules correlated with simulated spectra in gas phase and various solvents phase (polar, non-polar) computed by TD-SCF with IEFPCM level in the DFT as shown in Fig.6 [49]. The gas, water, DMSO, ethanol, chloroform, benzene and experimental spectra of maximum wavelength absorption, band gap, oscillation strength, large and small contributions are given in the Table5 [50,51]. The calculated band gap energies and λ_{\max} values are in gas phase shows 233.68, 191.63 nm (5.30, 6.47 eV). The solvent phases exhibit water→ 233.68, 191.63 nm (5.30, 6.47 eV), DMSO→ 234.67, 191.71 nm (5.28, 6.46 eV), ethanol→ 234.07, 191.73 nm (5.29, 6.46 eV), Chloroform→ 235.36, 192.17 nm (5.29, 6.45 eV) and Benzene→ 236.26, 192.49 nm (5.24, 6.44 eV) compared with experimental spectra 235, 189 nm (5.27, 6.56 eV) on the TTCPE molecules. The overall corresponding major contribution energy are H→L (58%) and HOMO→L+1 (65%), with electronic transition $\pi\rightarrow\pi^*$ successively. All of the spectral information from theoretical spectrum has been contrast and good match with experimental spectrum. In theoretically, the polar solvents have slightly larger band gap energy than non-polar solvents that illustrates the important biological activity of polar solvent molecules.



[Download: Download high-res image \(466KB\)](#)

[Download: Download full-size image](#)

Fig. 6. Experimental and theoretical UV-vis spectra on gas and various solvents.

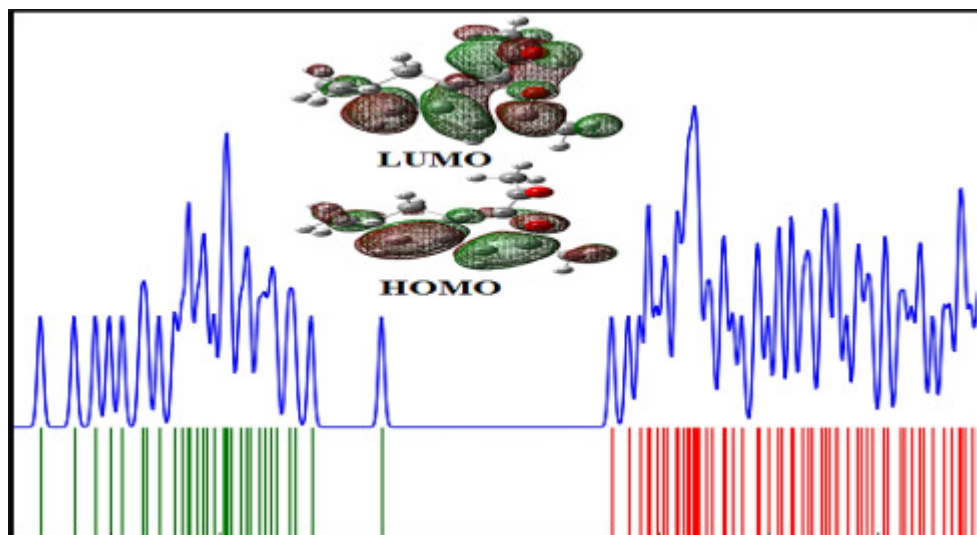
Table 5. UV-vis excitation energy and oscillator strengths on TTCPE.

Solvents	B3LYP hybrid 6-311++G (d, p)				Major Contributions Energy (%)	Minor Contributions Energy (%)
	Absorption band λ max (nm)	Energy cm^{-1}	Oscillation Strength (f)	Band gap		
Gas	258.45	38692.29	0.0004	4.79	H-3->L (19%), H-2->L (44%)	H-3->L+1 (3%), H-2->L+1 (6%),
	233.68	42794.46	0.7944	5.30	H->L (27%), H->L+1 (64%)	H-1->L (8%)
	191.63	52184.43	0.0596	6.47	H->L (57%), H->L+1 (23%)	H-1->L (2%), H->L+21 (2%)
Water	258.45	38692.29	0.0004	4.79	H-3->L (19%), H-2->L (44%)	H-3->L+1 (3%), H-2->L+1 (6%),
	233.68	42794.46	0.7944	5.30	H->L (27%), H->L+1 (64%)	H-1->L (8%)
	191.63	52184.43	0.0596	6.47	H->L (57%), H->L+1 (23%)	H-1->L (2%), H->L+21 (2%)
DMSO	258.62	38666.48	0.0004	4.77	H-3->L (18%), H-2->L (44%)	H-3->L+1 (3%), H-2->L+1 (6%),
	234.67	42613.79	0.8152	5.28	H->L (27%), H->L+1 (65%)	H-1->L (8%)
	191.71	52163.46	0.0594	6.46	H->L (58%), H->L+1 (23%)	H-1->L (2%), H->L+21 (2%)
Ethanol	258.93	38620.51	0.0004	4.78	H-3->L (18%), H-2->L (45%)	H-3->L+1 (2%), H-2->L+1 (6%),
	234.07	42721.87	0.8007	5.29	H->L (27%), H->L+1 (64%)	H-1->L (8%)
	191.73	52156.20	0.0599	6.46	H->L (57%), H->L+1 (23%)	H-1->L (2%), H->L+21 (3%)

Solvents	B3LYP hybrid 6-311++G (d, p)				Major Contributions Energy (%)	Minor Contributions Energy (%)
	Absorption band λ max (nm)	Energy cm^{-1}	Oscillation Strength (f)	Band gap		
Chloroform	261.47	38246.26	0.0004	4.74	H-3-> (13%), H-2->L (49%)	H-2->L+1 (6%), H-1->L (8%)
	235.36	42487.96	0.8169	5.29	H->L (27%), H->L+1 (64%)	H-1->L (2%),
	192.17	52036.83	0.0616	6.45	H->L (57%), H->L+1 (22%)	H->L+4 (2%), H->L+21 (3%)
Benzene	263.99	37880.89	0.0004	4.69	H-3->L (10%), H-2->L (52%)	H-2->L+1 (7%), H-1->L (8%)
	236.26	42326.65	0.8253	5.24	H->L (27%), H->L+1 (63%)	H-1->L (2%),
	192.49	51951.33	0.0633	6.44	H->L (57%), H->L+1 (22%)	H->L+2 (2%), H->L+4 (2%), H->L+21 (3%)
Experimental	235	-	-	5.27	-	-
	189	-	-	6.56	-	-

4.4.3. DOS analysis

The density of states (DOS) spectrum describe about charges interact with valance, conduction band and many energy states have been performed by using GaussSum 3.0 software with EWHM, which is filled orbital and empty orbital in the molecular structure [52,53]. The filled orbital is depicted as green, negatively charged (HOMO) and bonding interaction in the tetrahydrocyclopenta ($\text{C}_7\text{H}_4\text{O}_1$) has donor attached to the C_1 atom. The empty orbital express red colour, positively charged (LUMO) and non-bonding interaction in the ethanone ($\text{C}_2\text{H}_3\text{O}$) has receiver attached to the carbon C_3 as shows in Fig.7. The energy gaps seen in the DOS band spectra and HOMO - LUMO are exactly same and well correlated, respectively.



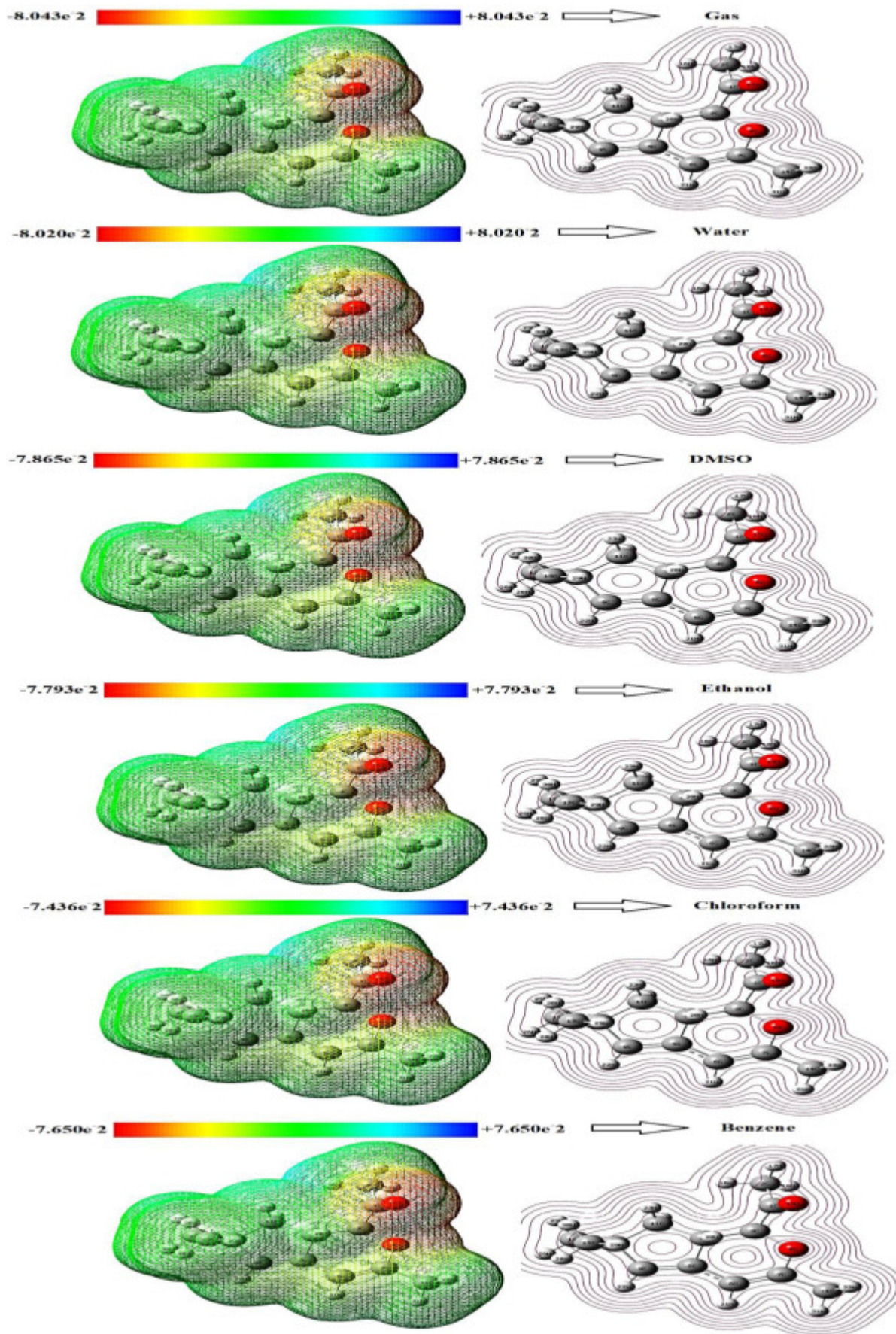
Download: [Download high-res image \(480KB\)](#)

Download: [Download full-size image](#)

Fig. 7. Density of states of CMIO.

4.5. MEP surface analysis

The MEP plot express about size, shape and electronic density, at each atom interaction with other atom through three dimensional ways on the molecular system. It is highly helpful for identifying the sites locations of nucleophilic, electrophilic reactivity based on colour shift and especially the properties of biomolecules, medications and physical, chemical qualities [[54], [55], [56]]. The MEP plot on TTCPE components was created optimized structure interpreted by GaussView 5.0 application as shown in Fig.8. The electrostatic potential plot of gas phase and various solvent phase colour ranges from $-8.043, -8.020, -7.950, -7.865, -7.793, -7.436 \times 10^{-2}$ a.u (appear in red code) to $8.043, 8.020, 7.950, 7.865, 7.793, 7.436 \times 10^{-2}$ a.u (exist in blue code) that potential rises towards in the order red, orange, yellow, green, cyan, and blue colour [57]. The local negative electrostatic potential occupied in oxygen atoms in gas and solvent phases represent as electrophilic reactive site (Donor) whereas the local positive electrostatic potential around in hydrogen atoms in gas and solvent phases indicates as nucleophilic reactive site (acceptor) while the localized zero electrostatic potential express in green surface area. The reactive sites express gas and water phase nearby same compare with other solvents both are related to well biological activity on TTCPE molecules successively.



[Download: Download high-res image \(3MB\)](#)

[Download: Download full-size image](#)

Fig. 8. MEP and contour surface plot on gas and various solvents.

4.6. Natural bond orbital (NBO)

The NBO analysis has powerful method to describe individual bond interaction, intra-inter molecular hydrogen bond interaction, charge transfer (donor-acceptor) or delocalization in electronic system are play important role in TTCPE molecules. The various second-order perturbative estimates the larger stabilization energy occupied (donor) orbital Lawis NBO measured in bond pair or lone pair and vacant (acceptor) orbital non-Lawis measured in anti-bonding or Rydberg are known as zeroth – order natural Lewis structure to the conjugation correction [58,59]. The large stabilization $E(2)$ values and the more electron density of donor and acceptor interaction in empty and filled orbital are basis of natural bond orbital (NBO) using to express Fock matrix in the second-order perturbation theory. The above mentioned all calculation performed by DFT/B3LYP process at level of 6-311++G(d,p) basis set as given in [Table6](#), respectively [60]. In the current investigations the number of donor-acceptor stabilization energy of strongly delocalization at 128.06kcal/mol has associated with donor (occupied orbital) $BD^*(2) C_6-C_7 \rightarrow BD^*(2) C_5-C_9$ acceptor (virtual orbital) interactions, which is maximum stabilized energy on TTCPE molecular system and the hyper conjugative interaction $BD(2) C_5-C_9 \rightarrow BD^*(2) C_6-C_7$, $BD(2) C_6-C_7 \rightarrow BD^*(2) C_5-C_9$, $LP(2) O_8 \rightarrow BD^*(2) C_6-C_7$, $LP(2) O_{15} \rightarrow BD^*(1) C_1-C_2$, $LP(2) O_{15} \rightarrow BD^*(1) C_1-C_3$, that donor, acceptor interaction corresponding with minimum stabilization of energy $E(2)$ values 16.56, 24.27, 35.01, 20.44, 21.03kcal/mol, respectively. The bonding - antibonding ($\sigma^* \rightarrow \sigma^*$) produce large amount of energy, which is carbon-carbon interaction and lone pair – antibonding ($LP(1) \rightarrow \sigma^*$) exhibit maximum amount of energy $O_8 \rightarrow C_6-C_7$ interaction which is related to towards pharmacy and biomedicine uses on TTCPE Compound [61].

Table 6. NBO Analysis of TTCPE Compound.

Donor	Acceptor	$E(2)$ kcal/mol	$E(j)-E(i)$ a.u.	$F(i,j)$ a.u.
BD (1) C_5-C_6	$BD^*(1) C_5-C_9$	7.01	1.41	0.08
BD (1) C_5-C_9	$BD^*(1) C_5-C_6$	7.39	1.40	0.09
BD (2) C_5-C_9	$BD^*(2) C_6-C_7$	16.56	0.31	0.06
BD (2) C_6-C_7	$BD^*(2) C_5-C_9$	24.27	0.34	0.08
BD (1) C_6-H_{21}	$BD^*(1) C_7-O_8$	7.51	0.88	0.07
LP (1) O_8	$BD^*(1) C_6-C_7$	6.69	1.23	0.08

Donor	Acceptor	E(2) kcal/mol	E(j)-E(i) a.u.	F(i,j) a.u.
LP (2) O ₈	BD*(2) C ₆ -C ₇	35.01	0.37	0.10
LP (2) O ₁₅	BD*(1) C ₁ -C ₂	20.44	0.65	0.10
LP (2) O ₁₅	BD*(1) C ₁ -C ₃	21.03	0.65	0.10
BD*(2) C ₆ -C ₇	BD*(2) C ₅ -C ₉	128.06	0.01	0.07

4.7. Drug-Likeness profile

The toxicity studies were done in PKCM database which depicts the ADME Property of the Compound had strong polarity and was not easily absorbed by the body [62]. The compound TTCPE satisfies the Lipinski 5 rule's which show molecular mass of 206 DA, Hydrogen bond donors were depicted of value 0, Hydrogen Bond acceptors of the compound is 2, the octanol water index shows 2.907 and molar refractivity index 63.217 are listed in Table 7 [63,64]. The ADME property of the compound are highlighted shows adsorption in skin permeability 2.492 and water soluble shows -3 values exhibit the absolute minimum that might be regarded as acceptable. The chemical's TPSA is substantially lower than the value that is deemed dangerous. According to the highlighted chemical parameters exhibits beneficial pharmacological qualities based on the criteria shared by pharmaceutical medications.

Table 7. Drug likeness properties of TTCPE.

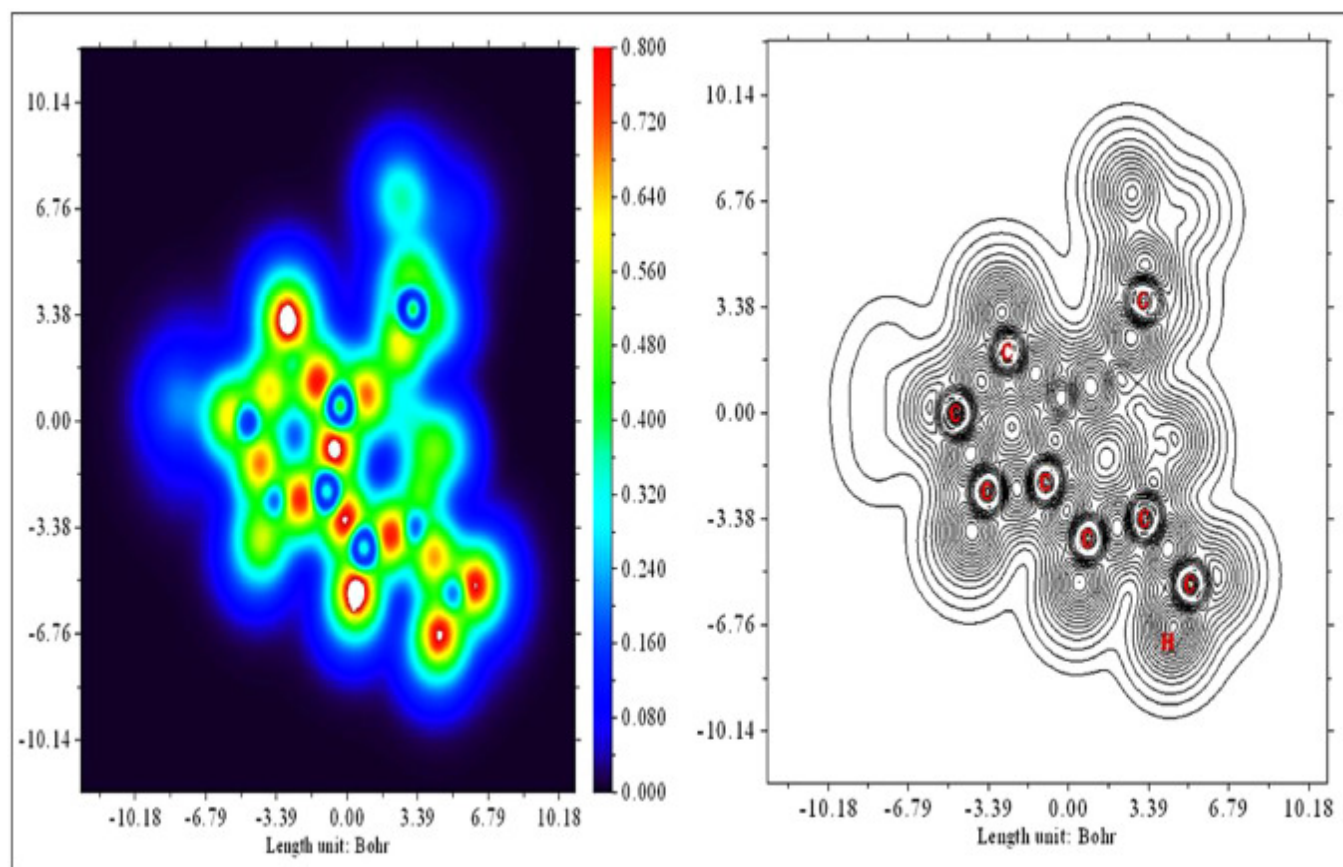
Properties	MW g/mol	LogP	HBD	HBA	Water Solubility	skin permeability	PSA(Å ²)
Lipinski 5 rule's	<500	<5	<5	<10	-	-	<130
C ₁₃ H ₁₈ O ₂	206	2.907	0	2	-3	2.492	63.21

4.8. Topological parameters investigation on TTCPE

4.8.1. LOL and ELF analysis

The investigation of covalent bond and amount of electron density interpreted by both methods are localised orbital locator (LOL) and electron localisation function (ELF) on the title compound [61]. Those are find areas of molecular region where each pair of electrons is more likely to be found [65]. In the present study colour filed projection map and contour

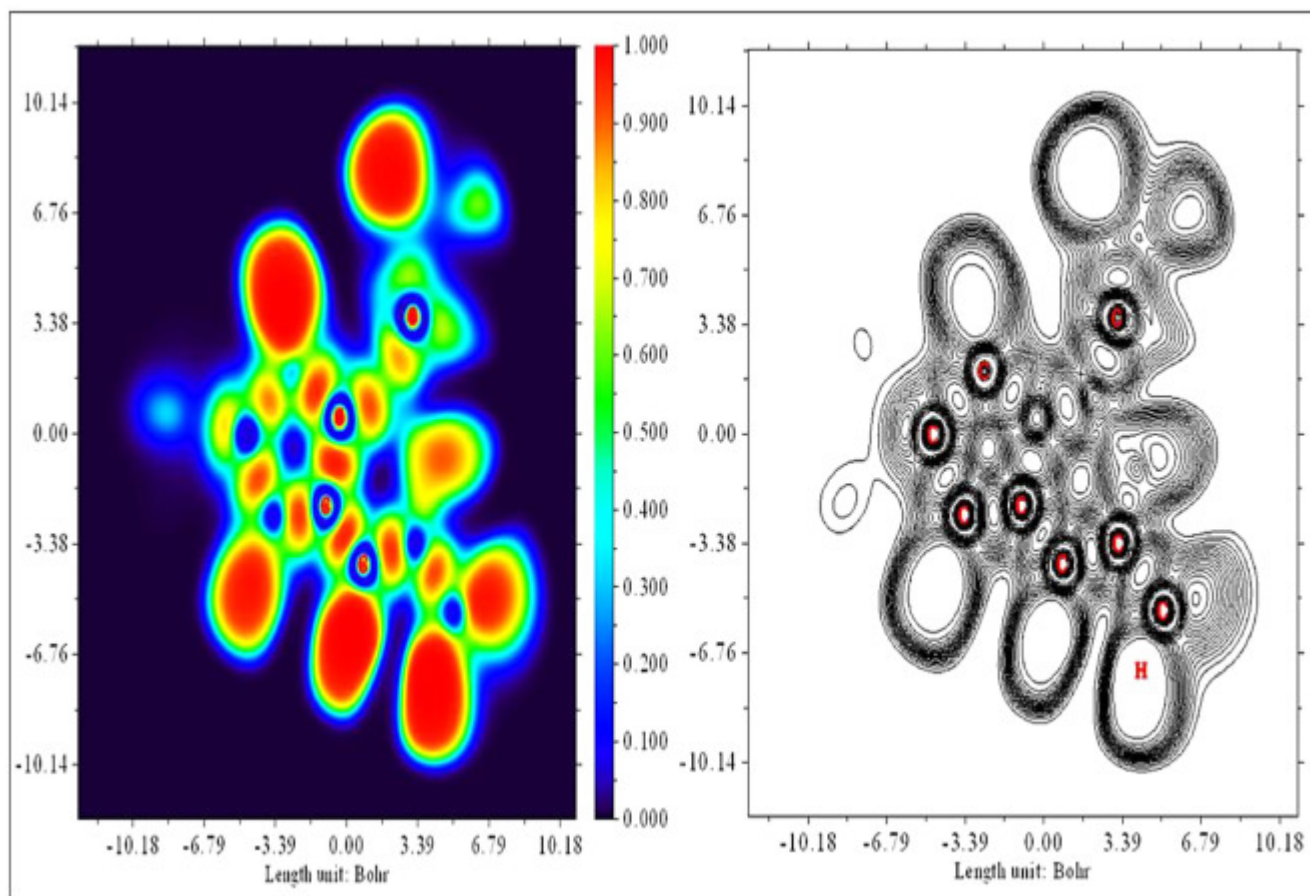
map of LOL, ELF obtained by Multiwfn 3.7 software on TTCPE molecules as shown in Fig. 9, Fig. 10 [66]. Generally, the ELF describes about electron pair of density and that plot configuration range from 0.5 to 1.0 which contain bonding, non-bonding localised electron pair and if the value is below > 0.5 which shows delocalised electron region on the title molecule. Similarly, the LOL describes the majority of localised orbital overlap and that map surface occurs in the range from 0 to 1.0 that contain where electron localization occurs over the density of electrons. The highest localisation of bonding and non-bonding electron pair of ELF, LOL are reported due to the presence of a covalent link and a lone pair of electrons in the surrounding area of hydrogen atoms. The delocalized of electrons pair of ELE, LOL are predicted around carbon atoms C_{14} , C_7 , C_6 , C_5 , C_9 , C_{10} , C_{11} , C_4 , C_2 in the tetrahydrocyclopenta structure due to their smaller values. Comparatively, the ELF gives a more detailed and perfect description than LOL gives on the TTCPE compound, respectively.



[Download: Download high-res image \(770KB\)](#)

[Download: Download full-size image](#)

Fig. 9. LOL (color-filled map with contour-Line Map) on TTCPE.



[Download: Download high-res image \(838KB\)](#)

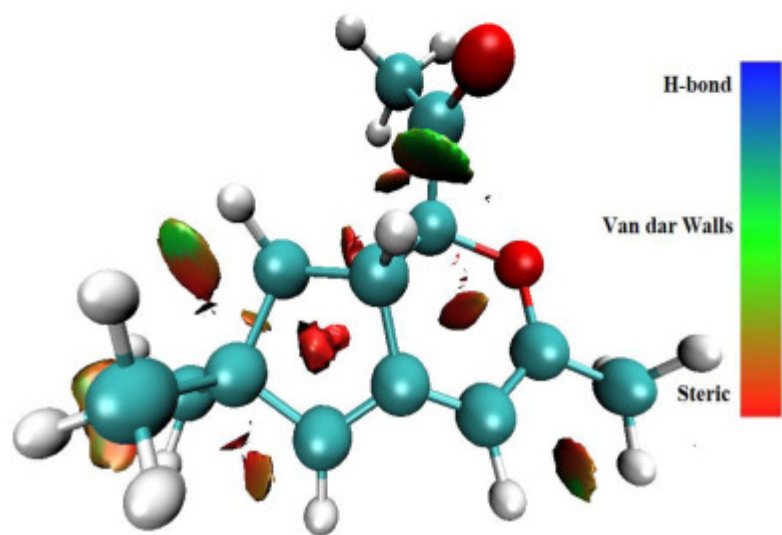
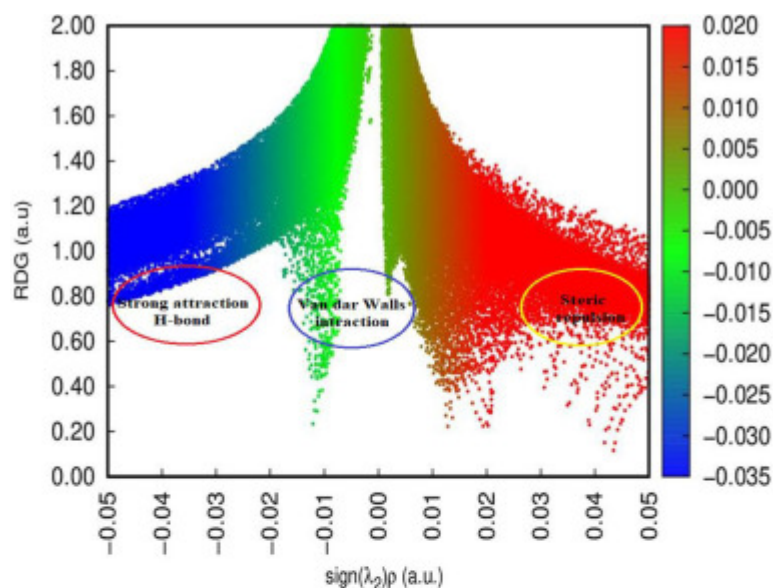
[Download: Download full-size image](#)

Fig. 10. ELF (color-filled map with contour-Line Map) on TTCPE.

4.8.2. RDG analysis

The reduced density gradient investigation of non-covalent interactions, which exhibit strong attraction, strong repulsion and neutral interaction of the molecular structure optimized by DFT/ B3LYP/6-311++G (d, p) technique [67]. The plot visualization based on electron density value in RDG parameter expresses information regarding strong and nature interaction and described by $\rho(r)$ indicate in graph as electron density, $(\lambda^2)\rho$ is difference between attraction and repulsion in RDG map [68]. The RDG graph illustrate about the sign of $(\lambda^2)\rho$ is greater than 0 its represent as red color range and strong steric effect repulsion, $(\lambda^2)\rho$ is less than 0 its express as blue with dark green color and strongest attraction and $(\lambda^2)\rho$ is nearby 0 its consider as green color and vandar walls interactions [[69], [70], [71]]. In the current study, the 2D scatters plot and RDG isosurface performed by Multiwfn 3.7 with VMD programs as shown in Fig. 11. From the RDG map red color in tetrahydrocyclopenta group positively charged (0.02–0.05) strong repulsion, dark green

color in ethanone group negatively charged (-0.02 - -0.05) strong attraction and green color in trimethyl neutrally charged (-0.01 - 0.01), which indicate all interactions are equally present as strong interaction in the title molecules successively.



Download: [Download high-res image \(634KB\)](#)

Download: [Download full-size image](#)

Fig. 11. RDG scatter graph with NCI on TTCEP.

4.9. Fukui function

The Fukui function has very fundamental and important element to characterize the reactivity and site-selectivity of organic molecular structure [20]. The Fukui function is local reactive variables commuted by using natural population analysis that indicates the way of electronic density to shift at certain place to gives or receives electrons that are much likely

come under an electrophilic or nucleophilic reactive [72]. The following statement evaluates the Fukui functions as $f^+(i) = P_i(N+1) - P_i(N) \rightarrow$ Nucleophilic attack $f^-(i) = P_i(N) - P_i(N-1) \rightarrow$ Electrophilic attack $f^0(i) = [P_i(N+1) - P_i(N-1)] / 2 \rightarrow$ Radical attack

Where p represent atomic charge i th ion location in positive ions ($N+1$), negative ions ($N-1$) and neutral (N) in the chemical substances and the signs of f^+ , f^- , f^0 indicates nucleophilic, electrophilic and radical attack interpreted hybrid B3LYP/6-311++G (d, p) approach. Additionally, the dual descriptor $\Delta f(r)$ can identify with an accurate sign in the locations of nucleophilic and electrophilic acts at certain location. This is described as the difference between the nucleophilic and electrophilic Fukui function and the dual descriptor were calculated by the equation of $\Delta f(r) = f^+(r) - f^-(r)$ [73]. In the current investigation, Fukui function, local softness and dual descriptor have been commuted based on NPA. The dual descriptor ($\Delta f(r) > 0$) exhibits nucleophilic sites whereas the dual descriptor ($\Delta f(r) < 0$) shows electrophilic sites as given in Table 8. The highest electropositive in the title molecules C2 > C14 > C13 > C12 > C11 > C8 > C6 > C9 > C4 > C5 are reported as reactivity order of nucleophilic attack. Similarly, the lowest electronegativity of TTCPE compound C4 > C11 > C15 > C6 > C8 > C2 > C9 are indicates reactive order of electrophilic attack while the radical attack reactivity order C2 > C14 > C12 > C8 > C15 > C11 > C4 > C5 > C7 successively. The local softness occurs as maximum electrophilic and nucleophilic reactive depending on local behavior in the TTCPE show good biological activity.

Table 8. To determine the local softness (S), Fukui Function (fr) and duel descriptor on TTCPE.

Atoms	Natural Population Charges			Fukui functions				Local Softness		
	0, 1 (N)	N+1 (-1, 2)	N-1 (1,2)	fi +	fi -	fi 0	fi	si+ fi+	si-fi-	si0 fi0
C1	0.58	0.33	0.28	-0.24	0.29	0.02	-0.54	-0.05	0.06	0.50
C2	-0.78	-0.38	-0.39	0.39	-0.38	0.02	0.78	0.08	-0.08	0.06
C3	0.02	0.01	0.05	-0.00	0.01	0.08	-0.01	-0.07	0.01	0.12
C4	-0.29	-0.13	-0.15	0.15	-0.14	0.04	0.29	0.03	-0.02	0.07
C5	-0.04	-0.05	0.01	0.03	-0.05	-0.01	0.09	0.09	-0.01	-0.07
C6	-0.36	-0.19	-0.00	0.16	-0.35	-0.09	0.52	0.04	-0.07	-0.02
C7	0.36	0.23	0.33	-0.13	0.03	-0.04	-0.16	-0.04	0.08	-0.06
C8	-0.53	-0.26	-0.15	0.26	-0.37	-0.05	0.64	0.03	-0.07	-0.12
C9	-0.21	-0.07	0.21	0.14	-0.42	-0.14	0.57	0.03	-0.08	-0.02

Atoms	Natural Population Charges			Fukui functions				Local Softness		
	0, 1 (N)	N+1 (-1, 2)	N-1 (1,2)	f _i +	f _i -	f _i 0	f _i	s _i + f _i +	s _i -f _i -	s _i 0 f _i 0
O10	-0.07	-0.03	-0.05	0.03	-0.01	0.08	0.05	0.06	-0.04	0.20
C11	-0.45	-0.22	-0.22	0.23	-0.22	0.04	0.45	0.04	-0.04	0.08
C12	-0.67	-0.33	-0.33	0.34	-0.34	0.02	0.69	0.07	-0.07	0.02
C13	-0.67	-0.33	-0.32	0.34	-0.35	-0.05	0.70	0.07	-0.07	-0.07
C14	-0.72	-0.35	-0.37	0.36	-0.34	0.07	0.70	0.07	-0.07	0.02
C15	-0.52	-0.24	-0.24	0.27	-0.27	-0.06	0.55	0.05	-0.05	-0.03
C16	0.25	0.11	0.12	-0.13	0.12	-0.09	-0.26	-0.02	0.02	-0.02
C17	0.26	0.11	0.14	-0.14	0.11	-0.01	-0.26	-0.03	0.02	-0.09
C18	0.25	0.11	0.13	-0.14	0.12	-0.01	-0.26	-0.02	0.02	-0.02
C19	0.22	0.10	0.12	-0.12	0.09	-0.01	-0.22	-0.02	0.02	-0.08
C20	0.26	0.12	0.14	-0.14	0.11	-0.01	-0.26	-0.02	0.02	-0.06
C21	0.24	0.10	0.13	-0.14	0.10	-0.01	-0.24	-0.02	0.02	-0.05
C22	0.23	0.09	0.12	-0.13	0.10	-0.01	-0.24	-0.02	0.02	-0.01
C23	0.24	0.11	0.13	-0.13	0.10	-0.01	-0.23	-0.02	0.02	-0.06
H24	0.23	0.11	0.12	-0.12	0.10	-0.07	-0.22	-0.02	0.02	-0.05
H25	0.23	0.10	0.13	-0.12	0.10	-0.01	-0.22	-0.02	0.02	-0.08
H26	0.23	0.10	0.12	-0.12	0.10	-0.01	-0.23	-0.02	0.02	-0.01
H27	0.23	0.11	0.12	-0.12	0.11	-0.07	-0.23	-0.02	0.02	-0.09
H28	0.23	0.10	0.12	-0.12	0.10	-0.01	-0.23	-0.02	0.02	-0.01
H29	0.23	0.11	0.12	-0.12	0.11	-0.02	-0.23	-0.02	0.02	-0.05
H30	0.23	0.10	0.13	-0.12	0.09	-0.01	-0.22	-0.02	0.01	-0.03
H31	0.24	0.11	0.13	-0.13	0.11	-0.01	-0.24	-0.02	0.02	-0.06
H32	0.25	0.11	0.15	-0.13	0.09	-0.01	-0.23	-0.02	0.02	-0.01
H33	0.25	0.11	0.15	-0.13	0.10	-0.01	-0.23	-0.02	0.02	-0.08

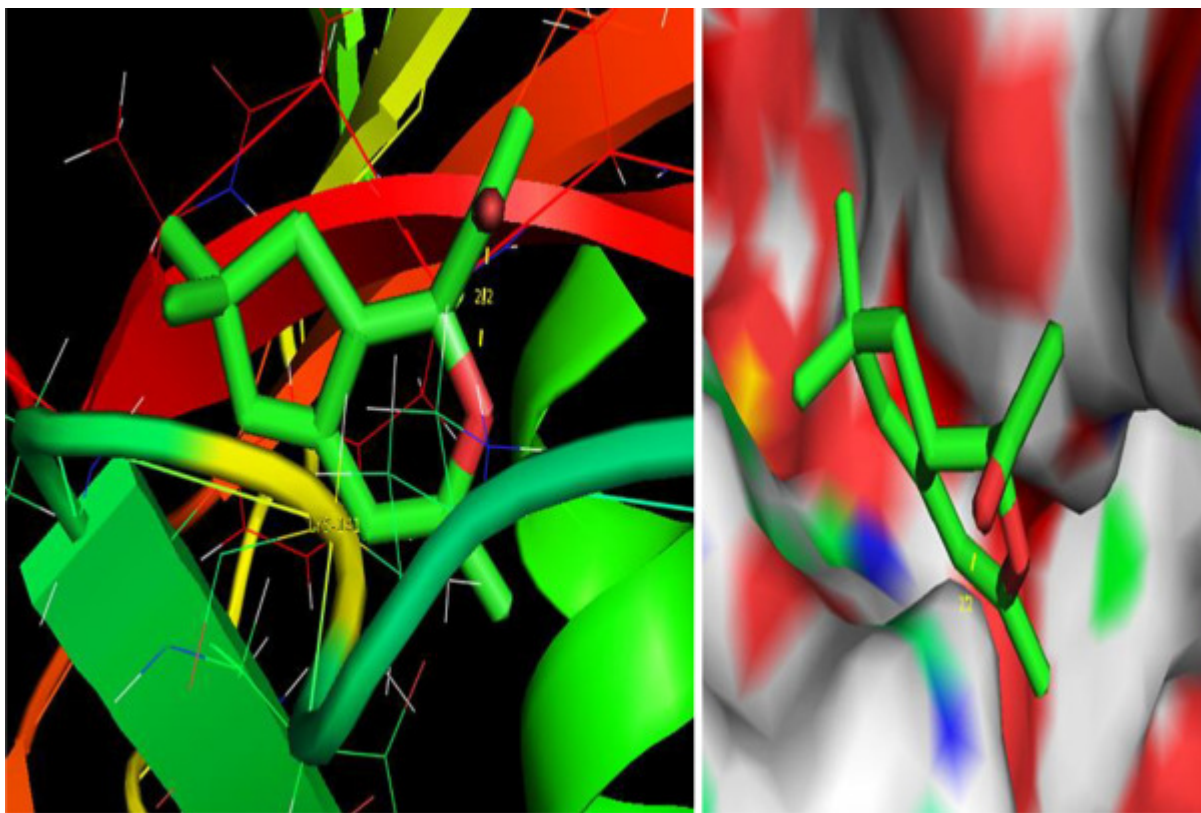
5. Molecular docking on TTCPE compound

The molecular modelling docking approach has been used to predict the behavior of small molecules interacts with binding site of target protein and also explain the basic biological mechanisms performed by AutoDock Tool 1.5.6 application [54]. In the current study, the synthesis of the TTCPE ligand selected the three active receptors. The first 1H8X protein against pancreatic cancer (Domain-swapped Dimer of a Human Pancreatic Ribonuclease Variant) which is classified under the enzyme Hydrolase ↗, the second protein 6R7T against melanoma cancer (Nanobody-complexed human Melanoma-Associated Antigen B1 (MAGEB1) which is classified under the enzyme Immune System ↗ and the third receptor 6DX5 against ovarian cancer (the viral OTU domain protease from Farallon virus) which is classified under the enzyme Immune System ↗ Hydrolase ↗. The Molview.org programme for translating PDB databases was used to prepare the ligands for the TTCPE molecules. The protein has been downloaded as a PDB file from the RCSB database for molecular docking execution. The AUTODOCK algorithm was ran on the CYGWIN-I platform. This software will generate GLG files and DLG files, which can be opened in WordPad and express bonded residues, bond distance (Å), intermolecular interaction (kcal/mol), estimated inhibition constant (µm), binding impact (kcal/mol) and reference RMSD (Å) of various active site protein are listed in [Table 9](#) [55,74]. The docking results reported the minimum binding energy of 1H8X, 6R7T and 6DX5 receptors exhibit -4.91, -5.46 and -5.83kcal/mol and the intermolecular energy were estimate -5.21, -5.75 and -6.13kcal/mol, respectively. The bonding distance and binding residues of 1H8X proteins shows LYS 141 in 2.2Å, 6R7T receptor expresses ARG 110 in 2.0Å and 6DX5 receptor reveal ASN 167 in 1.8Å, LEU 180 in 2.2Å amino acids as shown in [Fig. 12](#), [Fig. 13](#), [Fig. 14](#). The protein binds with title molecules by C₁—O₁₅, C₃—O₈—C₇ in tetrahydrocyclopenta ring plays important role for ligand-protein interactions. Amongst the all receptor, the maximum negative binding energy -5.83kcal/mol indicate effective drug of the 6DX5 protein against ovarian cancer which corresponds to a strong ligand-protein binding on TTCPE compound.

Table 9. The binding affinity of the proteins using AUTODOCK software.

Protein (PDB ID)	Bonded residues	Bond distance (Å)	Estimated Inhibition Constant (µm)	Inter molecular Energy	Binding impact (kcal/mol)	Reference RMSD (Å)
1H8X	LYS 141 (O... HZ1)	2.2	251.58	-5.21	-4.91	41.92

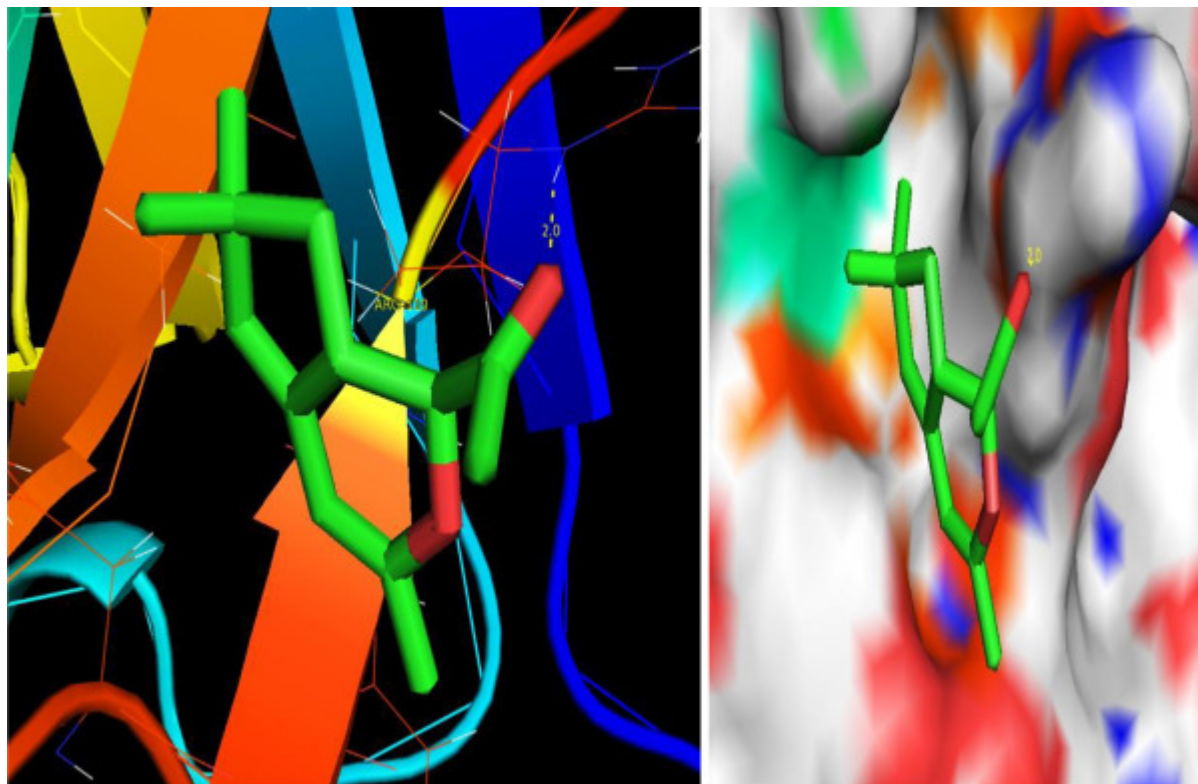
Protein (PDB ID)	Bonded residues	Bond distance (Å)	Estimated Inhibition Constant (μm)	Inter molecular Energy	Binding impact (kcal/mol)	Reference RMSD (Å)
6R7T	ARG 110 (O...HE)	2.0	100.33	-5.75	-5.46	35.32
6DX5	ASN 167 (O...HN) LEU 180 (O...HN)	1.8 2.2	53.36	-6.13	-5.83	48.05



[Download: Download high-res image \(787KB\)](#)

[Download: Download full-size image](#)

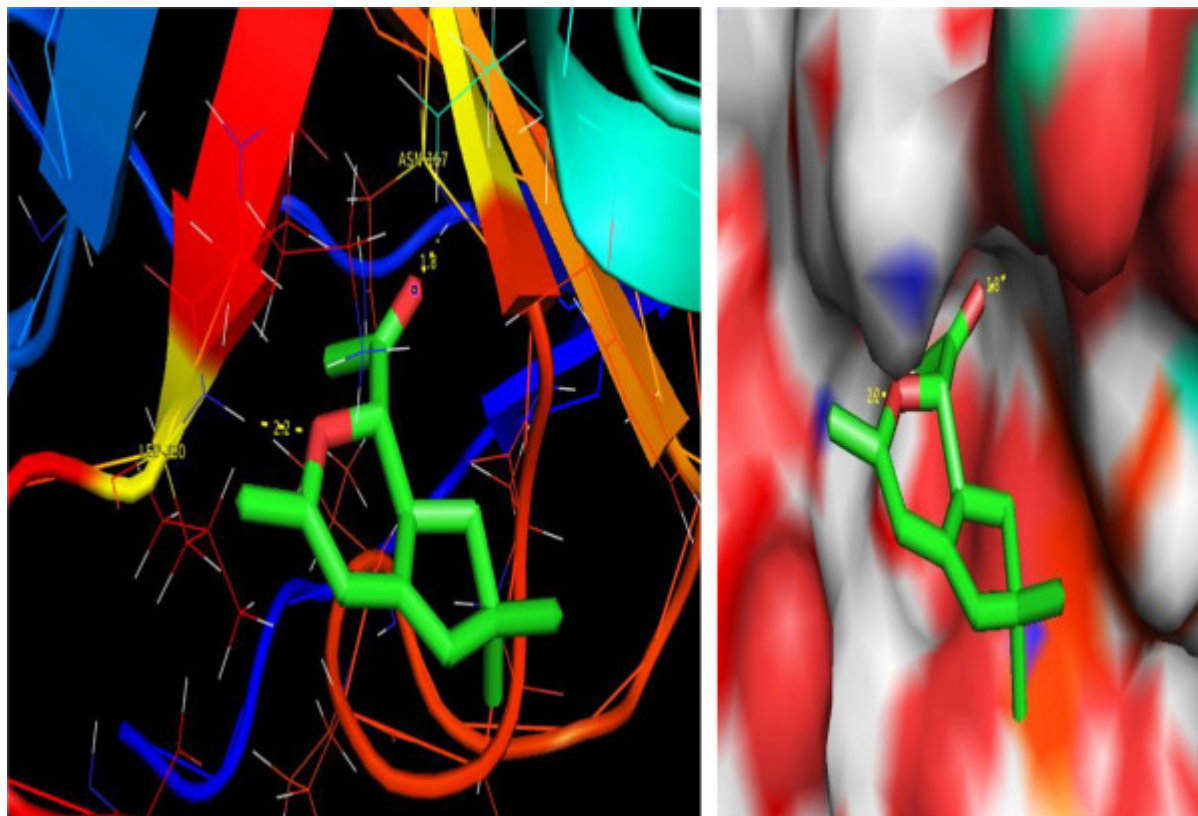
Fig. 12. Ligand-Docking complex are seen in the active site on 1H8X.



[Download: Download high-res image \(719KB\)](#)

[Download: Download full-size image](#)

Fig. 13. Ligand-Docking complex are seen in the active site on 6R7T.



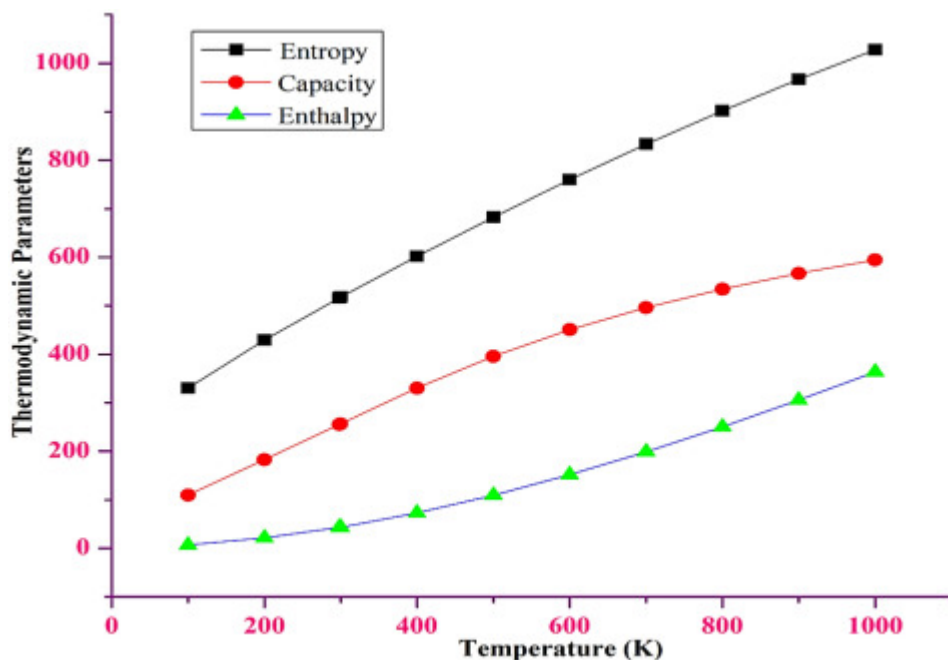
[Download: Download high-res image \(798KB\)](#)

[Download: Download full-size image](#)

Fig. 14. Ligand-Docking complex are seen in the active site on 6DX5.

5.1. Thermodynamics properties on TTCPE

The thermodynamic properties computed by stand-alone Perl-Script (thermol.pl) and the good accuracy of hybrid function B3LYP/6-311++G (d,p) set used to predict on TTCPE molecules to talk about their particular reactivity and thermodynamic stability as shown in [Fig. 15](#). In the current work, thermodynamic strength used to describe through various parameters of entropy, enthalpy and heat capacity displays in [Table 10](#) [75,76]. The result of S, C, H increases the values while the temperature also increased from 100 to 1000K due to the fact that molecules' temperatures increases their vibrational intensities amongst the particles and kinetic stability [77]. This demonstrates the good chemical for further studies and thermal stability of title molecule.



[Download: Download high-res image \(218KB\)](#)

[Download: Download full-size image](#)

Fig. 15. Thermodynamics parameters of TTCPE with temperature.

Table 10. Effect of temperature on TTCPE molecules by entropy, heat capacity and enthalpy.

T(K)	S(J/mol.K)	C(J/mol.K)	H(kJ/mol)
100	330.75	109.71	6.76
200	429.83	182.99	21.47
298.15	516.22	255.31	42.94
300	517.80	256.71	43.42
400	601.87	330.45	72.82
500	682.83	395.82	109.22
600	760	450.61	151.63
700	832.99	496.17	199.03
800	901.81	534.37	250.62
900	966.67	566.73	305.71

T(K)	S(J/mol.K)	C(J/mol.K)	H(kJ/mol)
1000	1027.84	594.34	363.80

5.2. Conclusion

The TTCEP ($C_{13}H_{18}O_2$) structure was synthesized from *Aeglemarmelos leaves* has been determined by the GC–MS data. The FT-IR spectrum was contrast to the calculated frequencies with PED% well matched. The PES revealed conformational study identified the strongest conformer and the optimized parameters (single, double bond) stability found and correlated with the XRD data. The high energy gap 10.494eV in gas and water showed well kinetic stability as best biological activity on TTCPE. The electronic spectra express gas and solvent ($\lambda_{max}=233.68, 191.63\text{ nm}$) are well contrast with UV–vis spectra ($\lambda_{max}=235, 189\text{ nm}$). The MEP surface exhibits electrophilic attack in oxygen atoms (repulsion) and nucleophilic attack in the hydrogen atoms (attraction). NBO computed effective charge transfer 119.54Kcal/mol and the reactive site were predicted by Fukui function using NPA charges. ADME results demonstrate the medicinal nature and Lipinski Rule of 5 estimated as drug likeness that suitable to act as an orally active potential drug in humans on TTCPE compound. LOL, ELF and RDG revealed bonding, non-bonding, interaction performed by Multiwfn 3.7 software. The docking studies exhibit good inhibitor against cancer activity receptors (1H8X, 6R7T and 6DX5) and comparatively, the minimum negative energy of the 6DX5 (–5.83kcal/mol) against ovarian cancer showed stable ligand–protein interactions.

CRedit authorship contribution statement

E. Dhanalakshmi: Conceptualization, Methodology, Validation, Formal analysis, Writing – original draft, Writing – review & editing, Visualization. **P. Rajesh:** Investigation, Supervision, Project administration, Writing – review & editing. **K. Arunkumar:** Formal analysis, Validation, Supervision, Methodology, Investigation. **T. Gnanasambandan:** Investigation, Resources, Supervision, Project administration, Writing – review & editing. **Noureddine ISSAOUI:** Methodology, Validation, Writing – review & editing. **K. Sudha:** Methodology, Validation, Writing – review & editing. **M. Raja:** Formal analysis, Validation, Supervision, Methodology, Investigation.

Declaration of Competing Interest

The authors declare that they have no known competing financial interests or personal relationships that could have appeared to influence the work reported in this paper.

[Recommended articles](#)

Data availability

Data will be made available on request.

References

- [1] A. Venthodika, N. Chhikara, S. Mann, M.K. Garg, S.A. Sofi, A. Panghal
Bioactive compounds of *Aegle marmelos* L., medicinal values and its food applications: a critical review
Phytother. Res., 35 (2020), [10.1002/ptr.6934](https://doi.org/10.1002/ptr.6934) [↗](#)
[Google Scholar](#) [↗](#)
- [2] S.E.Y. Rouholamini, S. Moghassemi, Z. Maharat, A. Hakamivala, S. Kashanian, K. Omidfar
Effect of silibinin-loaded nano-niosomal coated with trimethyl chitosan on miRNAs expression in 2D and 3D models of T47D breast cancer cell line
J. Herbs Spices Med. Plants, 46 (2017), pp. 524-535, [10.1080/21691401.2017.1326928](https://doi.org/10.1080/21691401.2017.1326928) [↗](#)
[Google Scholar](#) [↗](#)
- [3] Lu Sun, Z. Li, Z. Li, M. Gou, Z. Qian, F. Peng
Improving antitumor activity with N-trimethyl chitosan entrapping camptothecin in colon cancer and lung cancer
J. Nanosci. Nanotechnol., 15 (2020), pp. 6397-6404, [10.1166/jnn.2015.10736](https://doi.org/10.1166/jnn.2015.10736) [↗](#)
[Google Scholar](#) [↗](#)
- [4] S. Raheja, A. Girdhar, A. Kamboj, V. Lather, D. Pandita
Aegle marmelos leaf extract ameliorates the cognitive impairment and oxidative stress induced by intracerebroventricular streptozotocin in male rats
Life Sci., 221 (2019), pp. 196-203, [10.1016/j.lfs.2019.02.032](https://doi.org/10.1016/j.lfs.2019.02.032) [↗](#)
[View in Scopus](#) [↗](#) [Google Scholar](#) [↗](#)
- [5] R. Singh, A. Singh
Ethno-medicinal and pharmacological activities of *Aegle marmelos* (Linn.) Corr: a review
Pharma Innov., 8 (2019), pp. 176-181
[Crossref](#) [↗](#) [View in Scopus](#) [↗](#) [Google Scholar](#) [↗](#)

- [6] F. Mujeeb, P. Bajpai, N. Pathak
Phytochemical evaluation, antimicrobial activity, and determination of bioactive components from leaves of *Aegle marmelos*
Biomed. Res. Int. (2014), pp. 0-11, [10.1155/2014/497606](https://doi.org/10.1155/2014/497606) ↗
[Google Scholar](#) ↗
- [7] R. Babu Birudu, P. Pamulapati
Evaluation of biochemical changes in diabetic rats treated with *Aegle marmelos* (L.) methanolic leaf extract
Pharmacogn. J., 12 (2020), [10.4103/pr.pr_53_19](https://doi.org/10.4103/pr.pr_53_19) ↗
[Google Scholar](#) ↗
- [8] R. Tiwari, T. Tripathi, Y.A. Khan, A. Gupta, M. Dhobi, S. Srivastava, B. Singh, K. Shanker, V. Kalaiselvan, G.N Singh
Metabolite profiling, isolation of cyclic polyols, antioxidant and anti-inflammatory activities of *Aegle Marmelos*: NMR and GC-MS based metabolomics study
J. Herbs Spices Med. Plants, 27 (2020), pp. 68-82, [10.1080/10496475.2020.1786873](https://doi.org/10.1080/10496475.2020.1786873) ↗
[Google Scholar](#) ↗
- [9] U.K. Sahu, S. Sahu¹, S.S. Mahapatra, R.K. Patel
Synthesis and characterization of magnetic bio-adsorbent developed from *Aegle marmelos* leaves for removal of As(V) from aqueous solutions
Environ. Sci. Pollut. Res., 26 (2019), pp. 946-958, [10.1007/s11356-018-3643-1](https://doi.org/10.1007/s11356-018-3643-1) ↗
[View in Scopus](#) ↗ [Google Scholar](#) ↗
- [10] B. Veer, R. Singh
Phytochemical screening and antioxidant activities of *Aegle marmelos* leaves
Anal. Chem. Lett., 9 (2019), pp. 478-485, [10.1080/22297928.2019.1657946](https://doi.org/10.1080/22297928.2019.1657946) ↗
[View in Scopus](#) ↗ [Google Scholar](#) ↗
- [11] G. Sampath, M. Govarathanan, N. Rameshkumar, N. DaiViet, M. Krishnan, P. Sivasankar, N. Kayalvizhi
Ecofriendly biosynthesis metallic silver nanoparticles using *Aegle marmelos* (Indian bael) and its clinical and environmental applications
Appl. Nanosci., 13 (2023), pp. 663-674, [10.1007/s13204-021-01883-8](https://doi.org/10.1007/s13204-021-01883-8) ↗
[View in Scopus](#) ↗ [Google Scholar](#) ↗

- [12] P. Lalitha, A. Parthiban, V. Sachithanandam*, R. Purvaja, R. Ramesh
Antibacterial and antioxidant potential of GC-MS analysis of crude ethyl acetate extract from the tropical mangrove plant *Avicennia officinalis* L
S. Afr. J. Bot., 142 (2021), pp. 149-155, [10.1016/j.sajb.2021.06.023](https://doi.org/10.1016/j.sajb.2021.06.023) ↗
[View in Scopus ↗](#) [Google Scholar ↗](#)
- [13] M.J. Frisch, G.W. Trucks, H.B. Schlegel, G.E. Scuseria, M.A. Robb, J.R. Cheese-man, G. Scalmani, V. Barone, B. Mennucci, G.A. Petersson, H. Nakatsuji, M. Caricato, X. Li, H.P. Hratchian, A.F. Izmaylov, J. Bloino, G. Zheng, J.L. Son-nenberg, M. Hada, M. Ehara, K. Toyota, R. Fukuda, J. Hasegawa, M. Ishida, T. Nakajima, Y. Honda, O. Kitao, H. Nakai, T. Vreven, J.E. Peralta, F. Ogliaro, M. Bearpark, J.J. Heyd, E. Brothers, K.N. Kudin, V.N. Staroverov, R. Kobayashi, J. Normand, K. Raghavachari, A. Rendell, J.C. Burant, S.S. Iyengar, J. Tomasi, M. Cossi, N. Rega, J.M. Millam, M. Klene, J.E. Knox, J.B. Cross, V. Bakken, C. Adamo, J. Jaramillo, R. Gomperts, R.E. Stratmann, O. Yazyev, A.J. Austin, R. Cammi, C. Pomelli, J.W. Ochterski, R.L. Martin, K. Morokuma, V.G. Za-krzewski, G.A. Voth, P. Salvador, J.J. Dannenberg, S. Dapprich, A.D. Daniels, Farkas, J.B. Foresman, J.V. Ortiz, J. Cioslowski, D.J. Fox
Gaussian 09, Revision B.01
Gaussian Inc., Wallingfordl, CT (2010)
[Google Scholar ↗](#)
- [14] Naveen Kosar, Sana Noreen, Khurshid Ayub, Muhammad Imran, Tariq Mahmood
Structural, non-linear optical response and ultraviolet transparency of superalkalis (Li₃O, Na₃O, K₃O)-doped bowl shape silicon carbide nanoclusters
Inorg. Chem. Commun., 157 (2023), Article 111328
[View in Scopus ↗](#) [Google Scholar ↗](#)
- [15] M. Sohaib, H. Sajid, S. Sarfaraz, M.H.S.A. Hamid, M.A. Gilani, M. Ans, T. Mahmood, S. Muhammad, A.A. Mohammed, N.S. Sheikh, K. Ayub
Enhanced nonlinear optical response of alkalides based on stacked Janus all-cis-1,2,3,4,5,6-hexafluorocyclohexane
Heliyon, 9 (2023), p. e19325
[View in Scopus ↗](#) [Google Scholar ↗](#)
- [16] Simplice Koudjina, Wilfried G. Kanhounon, Gaston A. Kpotin, Affi Sopi Thomas, René Sawadogo, Abderrahmane Semmeq, Naveen Kosar, Michael Badawi, Tariq Mahmood, Guy Y.S. Atohoun
J. Mol. Graph. Model., 116 (2022), Article 108268
[View in Scopus ↗](#) [Google Scholar ↗](#)

- [17] Seema S. Khemalapure, Vinay S. Katti, Chidanandayya S. Hiremath, Sudhir M. Hiremath, Mahantesha Basanagouda, Shivaraj B. Radder
Spectroscopic (FT-IR, FT-Raman, NMR and UV-vis), ELF, LOL, NBO, and Fukui function investigations on (5-bromo-benzofuran-3-yl)-acetic acid hydrazide (5BBAH): experimental and theoretical approach
J. Mol. Struct., 1196 (2019), pp. 280-290, [10.1016/j.molstruc.2019.06.078](https://doi.org/10.1016/j.molstruc.2019.06.078) ↗
[View in Scopus ↗](#) [Google Scholar ↗](#)
- [18] N. Kanagathara, V.J. Thanigaiarasu, V. Sabari, S. Elangovan
Density functional theoretical computational studies on 3-methyl 2-vinyl pyridinium phosphate
Adv. Condens. Matter Phys. (2020), pp. 0-14, [10.1155/2022/6488234](https://doi.org/10.1155/2022/6488234) ↗
[Google Scholar ↗](#)
- [19] M. Lawrence, P. Rajesh, M. Thirunavukkarasu, S. Muthu
Solute-solvent interactions, electrostatic & covalent surface analysis, and pharmacokinetic studies via in-silico simulation on diethyl 3-hydroxyglutarate: anti-hypercholesterolemia activity
J. Mol. Liq., 382 (2023), Article 121940, [10.1016/j.molliq.2023.121940](https://doi.org/10.1016/j.molliq.2023.121940) ↗
[View in Scopus ↗](#) [Google Scholar ↗](#)
- [20] S. Janani, Hemamalini Rajagopal, S. Muthu, S. Aayisha, M. Raja
Molecular structure, spectroscopic (FT-IR, FT-Raman, NMR), HOMO-LUMO, chemical reactivity, AIM, ELF, LOL and molecular docking studies on 1-Benzyl-4-(N-Boc-amino)piperidine
J. Mol. Struct., 1230 (2021), [10.1016/j.molstruc.2020.129657](https://doi.org/10.1016/j.molstruc.2020.129657) ↗
[Google Scholar ↗](#)
- [21] P. Lalitha, A. Parthiban, V. Sachithanandam, R. Purvaja, R. Ramesh
Antibacterial and antioxidant potential of GC-MS analysis of crude ethyl acetate extract from the tropical mangrove plant *Avicennia officinalis* L
S. Afr. J. Bot., 142 (2021), pp. 149-155, [10.1016/j.sajb.2021.06.023](https://doi.org/10.1016/j.sajb.2021.06.023) ↗
[View in Scopus ↗](#) [Google Scholar ↗](#)
- [22] C.A. Ukwubile, A. Ahmed, U.A. Katsayal, J. Ya'u, S. Mejida
GC-MS analysis of bioactive compounds from *Melastomastrum capitatum* (Vahl) Fern. leaf methanol extract: an anticancer plant
Sci. Afr., 3 (2019), [10.1016/j.sciaf.2019.e00059](https://doi.org/10.1016/j.sciaf.2019.e00059) ↗
[Google Scholar ↗](#)

- [23] M.S. Padmashree, B. Roopa, R. Ashwathanarayana, Raja Naika
Antibacterial properties of *Ipomoea staphylina* Roem & Schult. plant extracts with comparing its preliminary qualitative phytochemical and quantitative GC-MS analysis
Trop. Plant Res., 5 (2018), pp. 349-369, [10.22271/tpr.2018.v5.i3.044](https://doi.org/10.22271/tpr.2018.v5.i3.044) ↗
[View in Scopus ↗](#) [Google Scholar ↗](#)
- [24] S. Selvaraj, P. Rajkumar, M. Kesavan, K. Thirunavukkarasu, S. Gunasekaran, N. Saradha Devi, S. Kumaresan
Spectroscopic and structural investigations on modafinil by FT-IR, FT-Raman, NMR, UV-vis and DFT methods
Spectrochim. Acta A Mol. Biomol. Spectrosc., 224 (2020), [10.1016/j.saa.2019.117449](https://doi.org/10.1016/j.saa.2019.117449) ↗
[Google Scholar ↗](#)
- [25] Gokhan Dikmen, Ozgür Alver
NMR, F.T.I.R., Raman and UV-vis spectroscopic investigation and DFT study of 6-bromo-3-pyridinyl boronic acid
J. Mol. Struct., 1099 (2015), pp. 625-632, [10.1016/j.molstruc.2015.05.063](https://doi.org/10.1016/j.molstruc.2015.05.063) ↗
[View in Scopus ↗](#) [Google Scholar ↗](#)
- [26] A. Rodger, M. Rodger
Molecular Geometry (1st Ed.), Elsevier Science (1995)
ISBN: 9781483106038
[Google Scholar ↗](#)
- [27] S. Sivaprakash, S. Prakash, S. Mohan, Sujin P. Jose
Quantum chemical studies and spectroscopic investigations on 22-amino-3-methyl-5-nitropyridine by density functional theory
Heliyon, 5 (2019), [10.1016/j.heliyon.2019.e02149](https://doi.org/10.1016/j.heliyon.2019.e02149) ↗
[Google Scholar ↗](#)
- [28] D.C. Fernandes, D.de A. Simoni, M. Rodrigues Jr, M.S. Santos, F. Coelho
Crystal structure of 3-(3,4,5-trimethoxyphenyl)-1,2,3,4-tetrahydrocyclopenta[*b*]indole-2-carboxylic acid
Acta Cryst., E71 (2015), pp. o395-o396, [10.1107/S2056989015008786](https://doi.org/10.1107/S2056989015008786) ↗
[View in Scopus ↗](#) [Google Scholar ↗](#)
- [29] Melvin J.G. Lesley, Koray Ozhan, Herman H.Y. Sung, Ian D. Williams
Trimethyl 4,400,40000-(ethene-1,1,2-triyl)tribenzoate

IUCrData, 5 (2020), [10.1107/S2414314620004174](https://doi.org/10.1107/S2414314620004174) ↗

[Google Scholar](#) ↗

- [30] Magdy A. Ibrahim, Shima Abdel Halim, N. Roushdy, Al-Shimaa Badran, Emad M. Ahmed, A.A.M. Farag

Fabrication, DFT modeling, and photoelectronic characterizations of novel pyridinylcarbonylquinoline for promising potential energy conversion

J. Mater. Res. Technol., 14 (2021), pp. 3092-3110, [10.1016/j.jmrt.2021.08.070](https://doi.org/10.1016/j.jmrt.2021.08.070) ↗

[Google Scholar](#) ↗

- [31] S. Saravanan, V. Balachandran

Quantum mechanical study and spectroscopic (FT-IR, FT-Raman, UV-visible) study, potential energy surface scan, Fukui function analysis and HOMO-LUMO analysis of 3-tert-butyl-4-methoxyphenol by DFT methods

Spectrochim. Acta A Mol. Biomol. Spectrosc., 130 (2014), pp. 604-620,

[10.1016/j.saa.2014.04.058](https://doi.org/10.1016/j.saa.2014.04.058) ↗

[View in Scopus](#) ↗ [Google Scholar](#) ↗

- [32] M. Smithaa, Y. Sheena Mary, Y. Shyma Mary, Goncagul Serdaroglu, Papia Chowdhury, Meenakshi Rana, H. Umamahesvari, B.K. Sarojini, B.J. Mohan, Rani Pavithrana

Modeling the DFT structural and reactivity studies of a pyrimidine -6-carboxylate derivative with reference to its wavefunction- dependent, MD simulations and evaluation for potential antimicrobial activity

J. Mol. Struct., 1237 (2021), [10.1016/j.molstruc.2021.130397](https://doi.org/10.1016/j.molstruc.2021.130397) ↗

[Google Scholar](#) ↗

- [33] P. Rajesh, S. Gunasekaran, T. Gnanasambandan, S. Seshadri

Molecular structure and vibrational analysis of Trifluoperazine by FT-IR, FT-Raman and UV-vis spectroscopies combined with DFT calculations

Spectrochim. Acta A Mol. Biomol. Spectrosc., 137 (2015), pp. 1184-1193,

[10.1016/j.saa.2014.08.100](https://doi.org/10.1016/j.saa.2014.08.100) ↗

[View in Scopus](#) ↗ [Google Scholar](#) ↗

- [34] T. Gnanasambandan, S. Gunasekaran, S. Seshadri

Experimental and theoretical study of p-nitroacetanilide

Spectrochim. Acta A Mol. Biomol. Spectrosc., 117 (2014), pp. 557-567, [10.1016/j.saa.2013.08.061](https://doi.org/10.1016/j.saa.2013.08.061) ↗

[View in Scopus](#) ↗ [Google Scholar](#) ↗

- [35] C. Charanya, S. Sampathkrishnan, N. Balamurugan

Quantum chemical computations, molecular docking, vibrational spectroscopic analysis, nonlinear optical properties and DFT calculation of 2- [(2,3-dimethylphenyl)amino]benzoic acid

Polycycl. Aromat. Compd., 41 (2021), pp. 1813-1834, [10.1080/10406638.2019.1700138](https://doi.org/10.1080/10406638.2019.1700138) ↗

[View in Scopus](#) ↗ [Google Scholar](#) ↗

- [36] M. Prabhakaran, A.R. Prbakaran, S. Gunasekaran, S. Srinivasan
Experimental and theoretical spectroscopic analysis, HOMO–LUMO, and NBO studies of cyanuric chloride

Spectrochim. Acta A Mol. Biomol. Spectrosc, 127 (2014), pp. 454-462,

[10.1016/j.saa.2014.02.040](https://doi.org/10.1016/j.saa.2014.02.040) ↗

[View in Scopus](#) ↗ [Google Scholar](#) ↗

- [37] S. Ghatfaoui, N. Issaoui, T. Roisnel, H. Marouani
Synthesis, experimental and computational study of a non-centrosymmetric material 3-methylbenzylammonium trioxonitrate

J. Mol. Struct., 1225 (2021), p. 129132, [10.1016/j.molstruc.2020.129132](https://doi.org/10.1016/j.molstruc.2020.129132) ↗

[Google Scholar](#) ↗

- [38] G. Karpagakalyaani, J. Daisy Magdalinea, T. Chithambarathanu
Comparative spectral (FT-IR, FT-Raman, UV) investigations, HOMO–LUMO, NBO and in-silico docking analysis of Nikethamide, niazid and 2-Mercaptonicotinic acid

J. Mol. Struct., 1252 (2022), [10.1016/j.molstruc.2021.132032](https://doi.org/10.1016/j.molstruc.2021.132032) ↗

[Google Scholar](#) ↗

- [39] A.S. Kazachenko, N. Issaoui, A. Sagaama, Y.N. Malyar, O. Al-Dossary, L.G. Bousiakou, A.S. Kazachenko, A.V. Miroshnokova, Z. Xiang
Hydrogen bonds interactions in biuret-water clusters: FTIR, X-ray diffraction, AIM, DFT, RDG, ELF, NLO analysis

J. King Saud University - Science, 34 (8) (2022), p. 102350, [10.1016/j.jksus.2022.102350](https://doi.org/10.1016/j.jksus.2022.102350) ↗

[View in Scopus](#) ↗ [Google Scholar](#) ↗

- [40] Towseef Ahmad Hajam, H. Saleem, M. Syed Ali Padhusa, K.K. Mohammed Ameen
Quantum mechanical study, spectroscopic (FT-IR, FT-Raman and UV–vis) study, NBO, NLO analysis and molecular docking studies of 2-ethoxy-4-(pyridine-2yliminomethyl)-phenol

Polycycl. Aromat. Compd., 42 (2022), pp. 4819-4842, [10.1080/10406638.2021.1896561](https://doi.org/10.1080/10406638.2021.1896561) ↗

[View in Scopus](#) ↗ [Google Scholar](#) ↗

- [41] S. Suresh, S. Gunasekaran, S. Srinivasan
Vibrational spectra (FT-IR, FT-Raman), frontier molecular orbital, first hyperpolarizability, NBO analysis and thermodynamics properties of Piroxicam by HF and DFT methods
Spectrochim. Acta A Mol. Biomol. Spectrosc., 138 (2015), pp. 447-459,
[10.1016/j.saa.2014.11.040](https://doi.org/10.1016/j.saa.2014.11.040) ↗
[View in Scopus](#) ↗ [Google Scholar](#) ↗
- [42] P. Rajesh, S. Gunasekaran, T. Gnanasambandan, S. Seshadri
Experimental, quantum chemical and NBO/NLMO investigations of pantoprazole
Spectrochim. Acta A Mol. Biomol. Spectrosc., 136 (2015), pp. 247-255,
[10.1016/j.saa.2014.09.029](https://doi.org/10.1016/j.saa.2014.09.029) ↗
[View in Scopus](#) ↗ [Google Scholar](#) ↗
- [43] Naveen Kosar, Tariq Mahmood
Outstanding NLO response of K3O@thia[n]circulenes; a DFT and molecular dynamics perspective
Phys. Scr., 98 (2023), Article 105249
[Crossref](#) ↗ [View in Scopus](#) ↗ [Google Scholar](#) ↗
- [44] Abdulrahman Allangawi, Naveen Kosar, Khurshid Ayub, Mazhar Amjad Gilani, Nur Hazimah Binti Zainal Arfan, Malai Haniti Sheikh Abdul Hamid, Muhammad Imran, Nadeem S. Sheikh, Tariq Mahmood
Decorating Mg12O12 nanocage with late first-row transition metals to act as single-atom catalysts for the hydrogen evolution reaction
ACS Omega, 8 (41) (2023), pp. 37820-37829
[Crossref](#) ↗ [View in Scopus](#) ↗ [Google Scholar](#) ↗
- [45] S. Kanchana, T. Kaviya, P. Rajkumar, M. Dhinesh Kumar, N. Elangovan, S. Sowrirajan
Computational investigation of solvent interaction (TD-DFT, MEP, HOMO-LUMO), wavefunction studies and molecular docking studies of 3-(1-(3-(5-((1-methylpiperidin-4-yl)methoxy)pyrimidin-2-yl) benzyl)-6-oxo-1,6-dihydropyridazin-3-yl)benzotrile
Chem. Phys. Impact, 7 (2023), [10.1016/j.chphi.2023.100263](https://doi.org/10.1016/j.chphi.2023.100263) ↗
[Google Scholar](#) ↗
- [46] Ramesh Rijal, Hari Prasad Lamichhane, Kiran Pudasainee

Molecular structure, homo-lumo analysis and vibrational spectroscopy of the cancer healing pro-drug temozolomide based on dft calculations

AIMS Biophys., 9 (2022), pp. 208-220, [10.3934/biophy.2022018](https://doi.org/10.3934/biophy.2022018) ↗

[View in Scopus](#) ↗ [Google Scholar](#) ↗

[47]

S. Liu

Conceptual density functional theory: Towards a New Chemical Reactivity Theory, Wiley (2022)

ISBN:9783527348435

[Google Scholar](#) ↗

[48]

J. Ebrahimian, M. Khayatkashani, N. Soltani, Qahtan A. Yousif

Catechin mediated green synthesis of Au nanoparticles: experimental and theoretical approaches to the determination HOMO-LUMO energy gap and reactivity indexes for the (+)-epicatechin (2S, 3S)

Arab. J. Chem., 15 (2022), [10.1016/j.arabjc.2022.103758](https://doi.org/10.1016/j.arabjc.2022.103758) ↗

[Google Scholar](#) ↗

[49]

M. Habib Rahuman, S. Muthu, B.R. Raajaraman, M. Raja, H. Umamahesvari

Investigations on 2-(4-Cyanophenylamino) acetic acid by FT-IR, FT-Raman, NMR and UV-vis spectroscopy, DFT (NBO, HOMO-LUMO, MEP and Fukui function) and molecular docking studies

Heliyon, 6 (2020), [10.1016/j.heliyon.2020.e04976](https://doi.org/10.1016/j.heliyon.2020.e04976) ↗

[Google Scholar](#) ↗

[50]

A. Saral, R. Shahidha, M. Thirunavukkarasu, S. Muthu

Molecular structure, spectral, computational, IEFPCM investigation, and topological study on the biologically potent; cardiotoxic drug 2-chloroquinolin-3-amine with structural optimization

Chem. Phys. Impact, 6 (2023), [10.1016/j.chphi.2023.100193](https://doi.org/10.1016/j.chphi.2023.100193) ↗

[Google Scholar](#) ↗

[51]

M. Thirunavukkarasu, G. Balaji, D. Shanthi, P. Prabakaran, Ahmad Irfan, S. Muthu

Experimental spectroscopic investigations, solute-solvent interactions, topological analysis and biological evaluations of N-(9-Fluorenylmethoxycarbonyloxy)succinimide: an effective agent in anti-breast cancer activity

J. Mol. Liq., 362 (2022), [10.1016/j.molliq.2022.119756](https://doi.org/10.1016/j.molliq.2022.119756) ↗

[Google Scholar](#) ↗

- [52] H. AlRabiah, S. Muthu, F.A.M. Al-Omary, A.M.S. Al-Tamimi, M. Raja, R. Raj Muhamed, A.A. El-Emam
Molecular structure, vibrational spectra, Nbo, Fukui Function, Homo-Lumo analysis and molecular docking study of 6-[(2-methylphenyl)sulfonyl]-5-propylpyrimidine-2,4(1h,3h)-dione
Maced. J. Chem. Chem., 36 (2017), [10.20450/mjccce.2017.1001](https://doi.org/10.20450/mjccce.2017.1001) ↗
[Google Scholar](#) ↗
- [53] N. Gunay, O. Tamer, D. Avci, E. Tarcanc, Y. Atalay
Molecular modelling, spectroscopic characterization and nonlinear optical analysis on N-Acetyl-DL-methionine
Rev. Mex. Fis., 66 (2020), pp. 749-760, [10.31349/RevMexFis.66.749](https://doi.org/10.31349/RevMexFis.66.749) ↗
[View in Scopus](#) ↗ [Google Scholar](#) ↗
- [54] M. Raja, R. Raj Muhamed, S. Muthu, M. Suresh
Synthesis, spectroscopic (FT-IR, FT-Raman, NMR, UV-visible), first order hyperpolarizability, NBO and molecular docking study of (E)-1-(4-bromobenzylidene)semicarbazide
J. Mol. Struct., 1128 (2017), pp. 481-492, [10.1016/j.molstruc.2016.09.017](https://doi.org/10.1016/j.molstruc.2016.09.017) ↗
[View in Scopus](#) ↗ [Google Scholar](#) ↗
- [55] C. Dabora Vincy, J.D. Deephlin Tarika, X.D. Divya Dexlin, A. Rathika, T. Joselin Beaula
Exploring the antibacterial activity of 1, 2 diaminoethane hexanedionic acid by spectroscopic, electronic, ELF, LOL, RDG analysis and molecular docking studies using DFT method
J. Mol. Struct., 1247 (2022), p. 131388, [10.1016/j.molstruc.2021.131388](https://doi.org/10.1016/j.molstruc.2021.131388) ↗
[Google Scholar](#) ↗
- [56] O. Noureddine, N. Issaoui, S. Gatfaoui, O. Al-Dossary, H. Marouani
Quantum chemical calculations, spectroscopic properties and molecular docking studies of a novel piperazine derivative
J. King Saud University - Science, 33 (2) (2021), p. 101283, [10.1016/j.jksus.2020.101283](https://doi.org/10.1016/j.jksus.2020.101283) ↗
[View in Scopus](#) ↗ [Google Scholar](#) ↗
- [57] G. Karpagakalyaani, J.D. Magdaline, T. Chithambarathanu
Comparative spectral (FT-IR, FT-Raman, UV) investigations, HOMO-LUMO, NBO and in-silico docking analysis of Nikethamide, niazid and 2-Mercaptonicotinic acid
J. Mol. Struct., 1252 (2022), [10.1016/j.molstruc.2021.132032](https://doi.org/10.1016/j.molstruc.2021.132032) ↗

[Google Scholar](#) ↗

- [58] F. Abbas, M.I Attia, S.K. Alghamdi, G.A. Khouqeer, Rageh K. Hussein
Spectroscopic, electronic properties analysis for 2, 6-Bis (phenylamino)-4-(iminophenyl) benzoquinone molecule and molecular docking clarification for its anticancer activity detected by strong inhibition of NQO1 enzyme
J. Mol. Struct., 1282 (2023), [10.1016/j.molstruc.2023.135231](https://doi.org/10.1016/j.molstruc.2023.135231) ↗

[Google Scholar](#) ↗

- [59] K.G. Sangeetha, K.K. Aravindakshan
Experimental, insilico, DFT studies of novel compound 2-{2-[(3,4-dimethoxyphenyl)methylidene] hydrazinecarbonothioyl}-N-methyl-N-phenylhydrazine-1-carbothioamide
Results Chem., 4 (2022), [10.1016/j.rechem.2022.100534](https://doi.org/10.1016/j.rechem.2022.100534) ↗

[Google Scholar](#) ↗

- [60] M. Vennila, R. Rathikha, S. Muthu, A. Jeelani, R.Niranjana Devi, Ahmad Irfan
Theoretical spectroscopic electronic elucidation with different solvents (IEFPCM model), biological assessment and molecular docking studies on Moroxydine-Antiviral drug agent
J. Mol. Liq., 355 (2022), [10.1016/j.molliq.2022.118946](https://doi.org/10.1016/j.molliq.2022.118946) ↗

[Google Scholar](#) ↗

- [61] S. Sambandam, B. Sarangapani, S. Paramasivam, R. Chinnaiyan
Molecular structure, vibrational spectral investigations (FT-IR and FT-Raman), NLO, NBO, HOMO-LUMO, MEP analysis of (E)-2-(3-pentyl-2,6-diphenylpiperidin-4-ylidene)-N-phenylhydrazinecarbothioamide based on DFT and molecular docking studies
Biointerface Res. Appl. Chem., 11 (2021), pp. 11833-11855, [10.33263/BRIAC114.1183311855](https://doi.org/10.33263/BRIAC114.1183311855) ↗

[View in Scopus](#) ↗ [Google Scholar](#) ↗

- [62] S.K. Alghamdi, F. Abbas, R.K. Hussein, A.G. Alhamzani, N.T. El-Shamya
Spectroscopic characterization (IR, UV-vis), and HOMO-LUMO, MEP, NLO, NBO analysis and the antifungal activity for 4-bromo-n-(2-nitrophenyl) benzamide—using DFT modeling and in silico molecular docking
J. Mol. Struct., 1271 (2023), [10.1016/j.molstruc.2022.134001](https://doi.org/10.1016/j.molstruc.2022.134001) ↗

[Google Scholar](#) ↗

- [63] R. Alnajjar, N. Mohamed, N. Kawafi

Bicyclo[1.1.1]pentane as phenyl substituent in atorvastatin drug to improve physicochemical properties: drug-likeness, DFT, pharmacokinetics, docking, and molecular dynamic simulation

J. Mol. Struct., 1230 (2021), [10.1016/j.molstruc.2020.129628](https://doi.org/10.1016/j.molstruc.2020.129628) ↗

[Google Scholar](#) ↗

- [64] J.N.C. Mishma, V.B. Jothy, A. Irfan, B. Narayana, S.N Kodlady, S. Muthu
Solvent potential effects (topological aspects, electron excitation), spectral characterization and biological attributes of NLO active 1-(2,4-dinitrophenyl)-2-((E)-3-phenylallylidene) hydrazine: multiple anti tuberculosis agent

J. Mol. Liq., 376 (2023), [10.1016/j.molliq.2023.121439](https://doi.org/10.1016/j.molliq.2023.121439) ↗

[Google Scholar](#) ↗

- [65] K. Arulaabaranam, S. Muthu, G. Mani, A.S. Ben Geoffrey
Speculative assessment, molecular composition, PDOS, topology exploration (ELF, LOL, RDG), ligand-protein interactions, on 5-bromo-3-nitropyridine-2-carbonitrile

Heliyon, 7 (2021), [10.1016/j.heliyon.2021.e07061](https://doi.org/10.1016/j.heliyon.2021.e07061) ↗

[Google Scholar](#) ↗

- [66] M. Lawrence, E. Isac Paulraj, P. Rajesh
Spectroscopic characterization, electronic transitions and pharmacodynamic analysis of 1-Phenyl-1,3-butanedione: an effective agent for antipsychotic activity

Chem. Phys. Impact, 6 (2023), [10.1016/j.chphi.2023.100226](https://doi.org/10.1016/j.chphi.2023.100226) ↗

[Google Scholar](#) ↗

- [67] A.S. Kazachenko, Y.N. Malyar, N.Yu. Vasilieva, V.S. Borovkova, N. Issaoui
Optimization of guar gum galactomannan sulfation process with sulfamic acid

Biomass Convers. Biorefin., 13 (6) (2021), pp. 1-10, [10.1007/s13399-021-01895-y](https://doi.org/10.1007/s13399-021-01895-y) ↗

[View in Scopus](#) ↗ [Google Scholar](#) ↗

- [68] F. Akman, A. Demirpolat, A.S. Kazachenko, Anna S. Kazachenko, Nouredine Issaoui, Omar Al-Dossary
Molecular structure, electronic properties, reactivity (ELF, LOL, and Fukui), and NCI-RDG studies of the binary mixture of water and essential oil of *Phlomis bruguieri*

Molecules., 28 (2023), [10.3390/molecules28062684](https://doi.org/10.3390/molecules28062684) ↗

[Google Scholar](#) ↗

- [69] V.S. Jeba Reeda, V. Bena Jothy, M. Asif, M. Nasibullah, N.S. Alharbi, G. Abbas, S. Muthu
Synthesis, solvent polarity(polar and nonpolar), structural and electronic
properties with diverse solvents and biological studies of (*E*)-3-((3-chloro-
4-fluorophenyl) imino) indolin-2-one

J. Mol. Liq., 380 (2023), [10.1016/j.molliq.2023.121709](https://doi.org/10.1016/j.molliq.2023.121709) ↗

[Google Scholar](#) ↗

- [70] A.S. Kazachenko, M. Medimagh, N. Issaoui, O. Al-Dossary, M.J. Wojcik, S.A. Kazachenko, A.V.
Miroshnokova, Y.N. Malyar

Sulfamic acid/water complexes (SAA-H₂O(1-8)) intermolecular hydrogen
bond interactions: FTIR,X-ray, DFT and AIM analysis

J. Mol. Struct., 1265 (2022), p. 133394, [10.1016/j.molstruc.2022.133394](https://doi.org/10.1016/j.molstruc.2022.133394) ↗

[View in Scopus](#) ↗ [Google Scholar](#) ↗

- [71] M. Medimagh, N. Issaoui, S. Gatfaoui, O. Al-Dossary, A.S. Kazachenko, H. Marouani, M.J.
Wojcik

Molecular modeling and biological activity analysis of new organic-
inorganic hybrid: 2-(3,4-dihydroxyphenyl) ethanaminium nitrate

J. King Saud University - Science, 33 (8) (2021), p. 101616, [10.1016/j.jksus.2021.101616](https://doi.org/10.1016/j.jksus.2021.101616) ↗

[View in Scopus](#) ↗ [Google Scholar](#) ↗

- [72] M. Sumithra, N. Sundaraganesan, R. Rajesh, V. Vetrivelan, V. Ilangovan, S. Javed, S. Muthu
Electron acceptor, excitation energies, oscillatory strength, spectroscopic
and solvent effects on 5-amino-4,6-dichloro-2-(propylthio) pyrimidine -
anticancer agent

Chem. Phys. Impact, 6 (2023), [10.1016/j.chphi.2022.100145](https://doi.org/10.1016/j.chphi.2022.100145) ↗

[Google Scholar](#) ↗

- [73] V.S. Jeba Reeda, V. Bena Jothy
Vibrational spectroscopic, quantum computational (DFT), reactivity (ELF,
LOL and Fukui), molecular docking studies and molecular dynamic
simulation on (6-methoxy-2-oxo-2H-chromen-4-yl) methyl morpholine-4-
carbodithioate

J. Mol. Liq., 371 (2023), [10.1016/j.molliq.2022.121147](https://doi.org/10.1016/j.molliq.2022.121147) ↗

[Google Scholar](#) ↗

- [74] M. Lawrence, P. Rajesh, A. Irfan, S. Muthu

Importance of solvent roles in molecular, electronic and dynamical properties, thermodynamic quantities, Mulliken charges, reactive analysis and molecular docking of 2-Bromo-1H-imidazole-4,5-dicarbonitrile

J. Mol. Liq., 388 (2023), [10.1016/j.molliq.2023.122744](https://doi.org/10.1016/j.molliq.2023.122744) ↗

[Google Scholar](#) ↗

- [75] A. Jumabaev, U. Holikulov, H. Hushvaktov, ISSAOUI Nouredine, A. Absanov
Intermolecular interactions in ethanol solution of OABA: raman, FTIR, DFT, M062X, MEP, NBO, FMO, AIM, NCI, RDG analysis

J. Mol. Liq., 377 (2023), Article 121552, [10.1016/j.molliq.2023.121552](https://doi.org/10.1016/j.molliq.2023.121552) ↗

[View in Scopus](#) ↗ [Google Scholar](#) ↗

- [76] P. Noudem, D. Fouejio, C.D.D. Mveme, F. Tchangnwa Nya, S.S. Zekeng
Electronic, nonlinear optical, UV-vis and NBO analysis of methyl methacrylate for optoelectronic and optical applications: DFT study and impact of conformation

Spectrochim. Acta A Mol. Biomol. Spectrosc, 303 (2023), Article 123267,

[10.1016/j.saa.2023.123267](https://doi.org/10.1016/j.saa.2023.123267) ↗

[View in Scopus](#) ↗ [Google Scholar](#) ↗

- [77] S. Aayisha, T.S. Renuga Devi, S. Janani, S. Muthu, M. Raja, S. Sevvanthi
DFT, molecular docking and experimental F.T.I.R., FT-Raman, NMR inquiries on “4-chloro-N-(4,5-dihydro-1H-imidazol-2-yl)-6-methoxy-2-methylpyrimidin-5-amine”: alpha-2-imidazoline receptor agonist antihypertensive agent

J. Mol. Struct., 1186 (2019), pp. 468-481, [10.1016/j.molstruc.2019.03.056](https://doi.org/10.1016/j.molstruc.2019.03.056) ↗

[View in Scopus](#) ↗ [Google Scholar](#) ↗

Cited by (0)

© 2023 The Authors. Published by Elsevier B.V.



All content on this site: Copyright © 2024 Elsevier B.V., its licensors, and contributors. All rights are reserved, including those for text and data mining, AI training, and similar technologies. For all open access content, the Creative Commons licensing terms apply.

